Martin Arriolabengoa, Eneko Iriarte, Arantza Aranburua, Iñaki Yusta, Lee J. Arnold, Martina Demuro, Alvaro Arrizabalaga

Reconstructing the sedimentary history of Lezetxiki II cave (Basque Country, northern Iberian Peninsula) using micromorphological analysis

Sedimentary Geology, 2018; 372:96-111

Final publication at http://dx.doi.org/10.1016/j.sedgeo.2018.05.006

Reconstructing the sedimentary history of Lezetxiki II cave (Basque Country, northern Iberian Peninsula) using micromorphological analysis

Martin Arriolabengoa[a,b,*], Eneko Iriarte[b,c], Arantza Aranburu[a,b], Iñaki Yusta[a], Lee J. Arnold[d], Martina Demuro[d], Alvaro Arrizabalaga[e]

[a] *Department of Mineralogy and Petrology, University of the Basque Country (UPV/EHU), Sarriena, 48940 Leioa, Spain.*
martin.arriolabengoa@ehu.es

[b] *ARANZADI Geo-Q Zentroa, Mendibile Kalea, 48940 Leioa, Bizkaia, Spain.*

[c] *Laboratory of Human Evolution, History, Geography and Communication Department, University of Burgos. Edificio I+D+i, Plaza de Misael Bañuelos, 09001, Burgos, Spain.*

[d] *School of Physical Sciences, Environment Institute, and Institute for Photonics and Advanced Sensing (IPAS), University of Adelaide, North Terrace Campus, Adelaide, SA, 5005, Australia*

[e] *Geography, Prehistory and Archaeology Department (UPV/EHU), Calle Tomás y Valiente, 01006 Vitoria-Gasteiz, Spain.*

Abstract

Micromorphological analysis is an invaluable research tool for reconstructing detailed depositional and post-depositional processes of cave infill sequences and for providing paleoenvironmental insight. In this work, we present the results of a micromorphological and mineralogical study of the sedimentary sequence at the Lezetxiki II cave (northern Iberian Peninsula). The cave forms part of the Lezetxiki archaeological complex which has yielded early Middle Palaeolithic tools and archaic human remains. We have identified three main clastic sedimentary processes as being significant at Lezetxiki II: 1) fluviokarst or runoff processes, which are characterised by yellow sandy illite-rich microfacies; 2) infiltration processes, which produce a massive red silty-clay vermiculite-rich microfacies; and 3) inwash processes, which generate a reworked illite and vermiculite rich silty sand microfacies. The most common post-depositional processes observed are calcite precipitation infilling pore spaces, and compression structures derived from specific vertical loading events. In order to improve the chronological framework of the sedimentary sequence at Lezetxiki II, we have revised previous radiometric and relative dating results from faunal and archaeological remains and have dated the lowermost stratigraphic level using single-grain thermally-transferred optically-stimulated luminescence dating. Sedimentation at the Lezetxiki II cave started during Marine Isotope Stage (MIS) 7 through fluviokarst processes. We interpreted that runoff prevailed during MIS 6, while soil infiltration processes became more significant toward the MIS 5 optimum. Gradually, inwash processes prevailed over infiltration until the end of the interglacial phase. During the following glacial phases, runoff and erosion dominated but were subsequently replaced by inwash processes during MIS 1.

Keywords: cave sedimentary processes; sedimentary petrology; single-grain dating; paleoenvironmental changes; Lezetxiki II cave.

1. Introduction

Karstic caves are complex geological environments in which a great variety of sedimentological processes can occur within a particularly limited area (Sasowsky and Mylroie, 2007; White, 2007). As in any other sedimentary environment, the sedimentary sequence in a cave represents records of local to regional paleoenvironmental changes that took place during its deposition (White, 2007). However, caves have been studied relatively less frequently than other sedimentary environments, and are generally absent or poorly documented in generic sedimentological books (e.g., Reineck and Singh, 1980; Reading, 1996; Nichols, 2009; Boggs, 2012). This is probably because of their limited accessibility and the large variability of factors involved in cave sedimentation. An exception to this is the study of speleothems, which have attracted the interest of the scientific community because of the accurate paleoclimatic information they can preserve (Fairchild and Baker, 2012), their spectacular morphology and their diverse mineralogy (Hill and Forti, 1997).

As Karkanas and Goldberg (2013) point out, cave sedimentary sequence studies are generally based on field description of sedimentary facies and grain-size characteristics with an emphasis on coarse-grained sediments and sediments transported by karstic aquifers (Bull, 1981; Bosch and White, 2004). However, much of the cave sediments are fine-grained deposits, and despite being an important source of information, they have been under-studied compared to other unconsolidated sedimentary bodies (van der Meer and Menzies, 2011). Over recent years, microstratigraphic studies of cave clastic sediments have been growing in importance, in part because sedimentological information is required to better understand accumulation processes of archaeological remains (Turk, 2011; Canti and Huisman, 2015). Karkanas and Goldberg (2013) reviewed cave sediment micromorphology studies published pre-2010, and summarised the main depositional and post-depositional processes detected in caves, as well as their paleoenvironmental and diagenetic interpretation. A number of recent works have been published that show existing correlations between cave depositional and post-depositional processes with climatic oscillations (Inglis et al., 2017; Morley et al., 2017; Nejman et al., 2018), landscape evolution (Ward et al., 2017) and diagenetic evidence (Stephens et al., 2017). However, most cave sedimentary sequences provide environmental information at a local scale, and normally additional geomorphological data from the surrounding area is needed to better understand the regional context.

During the past two decades several micromorphological studies have been carried out in cave clastic sediments at sites located within the Cantabrian Margin region (northern Iberian peninsula), where Lezetxiki II cave is located (Fig. 1). Courty and Vallverdú (2001) worked at El Mirón cave (located within the Cantabrian Margin) and another two caves, and found some correlation between environmental conditions and cave sedimentary process in a sequence spanning the late Upper Pleistocene to the early Holocene. Mallol et al. (2010) used micromorphology to show that limited post-depositional processes had affected the Esquilleu cave sequence since the Upper Pleistocene. Extreme flood events have been identified in speleothems from different caves located along the Cantabrian Margin, with chronologies spanning the Holocene and the Middle Pleistocene (Gázquez et al., 2014; González-Lemos et al., 2015a; 2015b). Lastly, Ballesteros et al. (2017) correlated MIS5d-c coarse-grained layers of a rhythmite deposits in the Torca la Texa shaft (Picos de Europa, Cantabrian Margin) with seasonal ice melting of surrounding glaciers, and fine-grained lamina forming by sedimentation of glacial flour during the non-melting season. These works have relatively limited geographical and chronological scope, and more data are now needed to improve our knowledge of the depositional and post-depositional processes affecting caves located in the Cantabrian Margin. Similarly, additional micromorphological information is needed to help better understand the climatic and geomorphological evolution of the region.

In this work we present a detailed study of the sedimentary sequence at Lezetxiki II cave (part of Lezetxiki archaeological complex, Arrasalte, Cantabrian Margin), which records sediment accumulation spanning the Middle Pleistocene through to the late

Holocene. The study is based in micromorphological analysis, and it follows on from previous work that investigated the provenance of the Lezetxiki II endokarstic sediments (Arriolabengoa et al., 2015). The aims of the current study are to (i) determine the sedimentary processes that took place within the cave during the various climatic cycles; (ii) understand how these sedimentary processes responded to ongoing environmental changes; and (iii) assess whether post-depositional events affected the sedimentary sequence through time. The results from this study will contribute towards our current knowledge on general cave sedimentary processes, aid in paleoenvironmental reconstruction at the local and regional scale, and provide a geological context for the archaeological and paleontological remains from the Lezetxiki archaeological complex, which is one of the most important sites in the northern Iberian Peninsula (Castaños et al., 2011; Arrizabalaga and Rios-Garaizar, 2012; Rofes et al., 2012; Villaluenga et al., 2012; Álvarez-Alonso, 2014; Arrizabalaga et al., 2014; Gómez-Olivencia et al., 2014; Rios-Garaizar et al., 2015a; Garcia-Ibaibarriaga et al., 2015).

2. Geological Context

2.1. Setting

The Lezetxiki II cave is situated in the northern margin of the Iberian Peninsula (Basque Country), near the village of Arrasate (Fig. 1), and within the upper Deba river basin, which discharges in the Cantabrian Sea. Within this basin, several caves preserve sedimentary sequences composed of distinct allostratigraphic units, where fluviokarstic processes, both erosive and sedimentary, prevailed during cold periods, and flowstone formation was dominant in temperate periods (Aranburu et al., 2015).

The Lezetxiki II cave is part of the Lezetxiki archaeological complex and is formed within the Aptian-Albian stratified reef limestones (García-Mondéjar, 1990; EVE, 1992), which are traversed from north to south by the Bostiturrieta watercourse (Fig. 1). At least nine caves have been documented along the valley. The layout of these caves, as well as their phreatic geomorphologies in the horizontally developed galleries, suggest the presence of two cave levels in the Bostiturrieta valley (Expósito et al., 2015) that formed during pauses in base-level lowering. The upper level is situated at 20-30 m above the current stream level, while the lower cave level is equivalent to that of the stream. Three types of soils have been identified in the Bostiturrieta valley (Fig. 1b), and these represent the source materials (i.e., surface clastic sediments) that were remobilised and then redeposited inside the cave (Fig. 1). These include: 1) soils formed above siliciclastic rocks (S_1), which, in a steep landscape, suffer relatively continuous erosion and soil rejuvenation (Velde and Meunier, 2008), and so are relatively richer in illite clay mineral; 2) soils above limestones (S_2), which suffer less erosion than S_1, and so are relatively richer in vermiculite, a pedogenic clay mineral formed from illite through loss of potassium; and, 3) a *terra rossa*-type soil (S_3), which forms above limestone and is almost unaffected by erosion, and is therefore, the soil with the richest vermiculite mineral content (Arriolabengoa et al., 2015).

2.2. Lezetxiki Archaeological Site

The Lezetxiki archaeological site complex is located in the upper cave level, approximately 25 m above the current stream, between the entrance of the Leibar cave and the end chamber of the Iturralde cave (Fig. 2). Both Leibar and Iturralde caves are actually part of the same cave system. However, the galleries connecting them were completely filled by sediments and they have therefore been treated as two separate caves. The sedimentary infill separating these two caves contains the archaeological and paleontological remains that make up the Lezetxiki site, where sedimentation began in the Middle Pleistocene (Arrizabalaga, 2006).

The site was first excavated from 1956 to 1968 (Barandiarán and Altuna, 1970) and then re-excavated from 1996 to 2016 (Arrizabalaga et al., 2004; Arrizabalaga, 2006). The second phase of fieldwork extended Barandiarán's first excavation laterally (Fig. 2), and also included the opening of the Lezetxiki II cave pit, which was excavated between 2001 and 2011. The original trench excavated by Barandiaran starts from the so called "tunnel of Lezetxiki" and ends ~10 m below it, at the entrance of the Leibar cave (Fig. 2). The sedimentary sequence of this trench is divided into eight stratigraphic levels (Altuna, 1972). A *Homo heidelbergensis* humerus was found at this site (i.e., Leibar entrance), but its exact stratigraphic ascription is unknown (Basabe, 1966; Arrizabalaga, 2006). The main chronological study undertaken at Lezetxiki, which included ESR dating, as well as alpha and gamma spectrometry, dating of bones, produced uncertain results, and the most relevant information obtained from that study is that level VII (second level starting from the base of the sequence) must be younger than 260 ka (Falguères et al., 2005/2006). The authors reasoned that meteoric waters percolated the sediment and contaminated the dated bone samples, thus increasing their apparent age (Falguères et al., 2005/2006).

The trench excavated by Arrizabalaga (2nd excavation; Fig. 2) is 8 m deep, but work is currently ongoing and final results regarding its stratigraphy and chronology are not yet available. Villaluenga et al. (2012) studied the macro-fauna remains from levels L, M, N and O (early Upper Pleistocene) of the 2nd excavation (Fig. 2), which are situated 5-6 m below the surface. A roof collapse occurred during the formation of these levels, separating the stratigraphic sequence into two different sedimentary environments: the upper part of the stratigraphy is classed as a rockshelter environment, while the lower part is classed as a cave environment.

Lezetxiki II is a small sediment-filled cave (6 m long and 3 m wide) that was originally excavated after the discovery that the cave was connected directly to the Leibar section. A trench of 4 x 1 m in area, and 3 m deep was excavated (Figs. 2, 3), until the presence of large limestone boulders impeded any further work. Lezetxiki II is topographically paired with the lower part of the other two excavation areas at Lezetxiki (Fig. 2), but the correlation between the various levels among the three trenches is still part of ongoing work. In this sense, the sedimentary context obtained in the present work will provide valuable information for improved correlations of the various infill sequences at Lezetxiki.

2.3. The Lezetxiki II cave stratigraphy

A sedimentary record of ca. 3.9 m was obtained from the excavated trench (Fig. 3). The sedimentary record encompasses eleven major lithostratigraphic levels - labelled from the base upwards, as K to A - and two main erosive surfaces (Fig. 3; Table 1). The bottom of the sequence is characterized by allochthonous fluviokarst sediments (levels K and J). With the exception of levels H, E and D, the higher levels are fine-grained deposits and have a massive structure. Levels H and E are also fine-grained levels, but level H is additionally composed of speleothem fragments, while in level E clastic sediments are cemented by calcium carbonate. Level D is the only *in situ* flowstone level of the sequence, and has been dated to 74 ka using uranium series analysis by alpha spectrometry (Falguéres et al., 2005/2006). Occasionally, subangular limestone boulders can be found randomly distributed along the sequence, which correspond to episodic cave roof breakdown events.

Arriolabengoa et al. (2015) were able to find two main sources for the clastic sediments using mineralogical and geochemical analysis of the cave sediments, and similar analyses performed on soils and rocks from the surrounding valley, as follows: i) the siliciclastic rocks of the upper valley and their soils (S_1) were carried to the cave by fluviokarstic processes and enriched the level in illite mineral. This process was dominant in level K, but decreased in importance in levels I, E and C; and ii) soils formed on limestone (S_2 and S_3) were eroded and introduced into the cave through the epikarst via infiltration processes, enriching some levels with vermiculite mineral. This process prevailed in level H, and to a lesser extent in levels G and B. The rest of the clastic sedimentary levels (levels J and F) preserve similar illite and vermiculite composition, and were interpreted as being affected equally by both processes (i.e., fluviokarst and infiltration).

3. Methods

The principal method used in this work is micromorphological analysis. However, we also present mineralogical data obtained by X-ray diffraction (XRD) in Arriolabengoa et al. (2015), since this helps with interpreting microfacies and sedimentary processes, and provides additional environmental information. Finally, we present new chronological data for level K obtained using single-grain thermally transferred optically stimulated luminescence (TT-OSL) dating of sedimentary quartz.

The micromorphological study focused on five unaltered sediment samples taken from levels I, H, G, F and B, including the contact between the levels (Fig. 3). Sampling was performed using aluminium kubiena boxes (7 cm wide and 13 cm long, taken vertically). Levels K, J and E could not be sampled due to the presence of a large number of pebbles. Level C was not sampled because of the fragile, non-cohesive nature of the sediment and level A was not studied because it is the modern altered surface layer. Thin sections were produced in the SCT Micromorphology and Image Analysis Laboratory at University of Lleida using the protocol developed by Benyarku and Stoops (2005). The thin sections were studied using an Olympus BH2 petrographic microscope equipped with an Olympus DP10 digital camera and Nikon Elements imaging software. Thin sections were described according to terminology used in soil micromorphology (Bullock et al., 1985; Stoops, 2003) and classical sedimentary petrology studies: these included descriptions of microfabric, microfacies and microstructure, grain size and shape, composition and distribution of skeleton grains and groundmass.

Mineralogical characterization of the sedimentary record was performed after obtaining one representative sample of loose sediment from each level. Due to the thickness of levels K and F, three samples were obtained for each at these two levels (Arriolabengoa et al., 2015) (Fig. 3). Whole-rock mineralogy was determined by powder X-ray diffraction (XRD) using a Bruker D8 Discover diffractrometer with DAVINCI design and the DIFFRACplus basic EVA software with ICDD database, at the Science and Technology Park in Burgos University. Air-dried samples were sieved at 2 mm, finely ground in an agate mortar to less than 63 µm particle size and processed using a continuous scan range of 2-80 °2θ with Cu Ka radiation (ceramic X-ray tube KFL-Cu, 40 kV, 40 mA) with a programmable divergence slit, and a LynxEye detector.

Semi-quantitative estimations were calculated from peak areas on XRD patterns. The clay fraction (<2 μm) mineralogy was identified with a PANalytical X'Pert Pro diffractometer at the Research Facilities (SGIker) of the University of the Basque Country. The samples were first decarbonated by treatment with 0.1 M HCl, washed several times with deionized water to avoid calcium chloride precipitation and the clay fraction was collected by centrifugation. The oriented aggregates were prepared by carefully pipetting the clay suspension onto glass slides that later were placed in a glass dessicator for 24 h with ethylene glycol solvent. Thermal treatments at 300°C and 550°C were also applied to identify the clay minerals following the procedures detailed in Arostegui et al. (2006). After each treatment step, the glass slides were measured by XRD with CuKa radiation (40 kV, 40 mA), graphite monochromator, a programmable divergence slit, and a PIXcel detector.

In order to obtain a better chronological understanding of the sedimentary sequence, a sediment sample (LZ12-6) was collected from level K for single-grain thermally transferred optically stimulated luminescence (TT-OSL) dating (e.g., Arnold and Demuro, 2015; Demuro et al., 2015). Single-grain TT-OSL provides an estimate of when sedimentary quartz grains were last exposed to light prior to burial at the site. This technique also offers the advantage of establishing extended-range depositional chronologies that exceed the traditional upper age limits of quartz OSL dating (Arnold et al., 2015). The TT-OSL sample was dated at the CENIEH Luminescence Dating Laboratory, Burgos (Spain). Equivalent dose (D_e) values were determined for individual quartz grains using the instrumentation, single-aliquot regenerative-dose (SAR) procedure and TT-OSL quality assurance criteria outlined in Arnold et al. (2014). The environmental dose rate for LZ12-6 was estimated using a combination of *in situ* field gamma spectrometry and low level beta counting, taking into account cosmic ray contributions (Prescott and Hutton, 1994), an assumed minor internal alpha dose rate (Bowler et al., 2003), beta-dose attenuation and present-day water content.

4. Results

4.1. Micromorphology

In general terms, studied levels show a massive microstructure and porphyric coarse-fine (*c/f*) related distribution. However, there are differences between the type of fine and coarse sediment that characterizes each microfacies. The main micromorphological features are summarised in Table 2. It should be noted that some fissure type cracks could have developed during the sampling or preparation stages.

4.1.1. Level I

Level I has a massive microstructure and heterogeneous groundmass. The heterogeneous aspect of the microfacies in this level is due to poor mixing of two different sediment types: 1) a yellow sandy sediment (YSS) with greater content of medium-size quartz sand and yellow clays (Fig. 4a); and 2) reddish silty sediment (RsS), with less sand, richer in anorthic ferruginous nodules and red clays (Fig. 4a). Skeleton grain components are poorly sorted and are made up of rounded equidimensional opaque minerals 0.1-1.0 mm in size, aggregates of rip-up clasts, sand and granules that are 0.1-2.8 mm in size (Fig. 4b), <4 mm-diameter lutite pebbles with blade to rod shape, flat or rounded morphology and non-eroded microfauna bone fragments. Some bones are chemically altered (Fig. 4d), forming a secondary phosphate mineral precipitate as discussed by Karkanas et al. (2000). The porosity is low (10%)

and the pores are characterised by vughy and fissure types (Fig. 4a). In the upper part of the level, the pores are sometimes partially filled with calcite acicular crystals in a radial arrangement (Fig. 4c).

4.1.2. Level H

There are two microstructures in Level H. The first microstrucure has a breccia-type structure and bimodal fabric (Figs. 5, 6a) formed by subangular speleothem fragments. Some of the fragments are in a sub-horizontal position, forming a pseudo-linear structure which reflects the bedding (Fig. 5). The skeleton grain is made up of flowstone-type speleothem fragments that are up to 1 cm thick. Most are altered, corroded and micritized, while a few preserve their original dendritic crystalline texture. Most of the speleothem fragments are upturned (Fig. 6a), others are on their side and a few are in the original growth position (Fig. 5). In addition to the speleothem fragments, some microfaunal bone remains and anorthic ferruginous grains can be observed. About the groundmass, two types of fine-sediments can be differentiated (Fig. 6b). The most common is a red homogeneous groundmass (RsS) (Fig. 6a, b), however, in the lower part of Level H there are two discontinuous intercalated layers of yellow sandy-silt sediment (YSS) (Figs. 5, 6).

The second microstructure is matrix-supported by RsS sediment (Fig. 6c, d), which gives it a massive microstructure and reddish homogeneous fine-sediment microfacies. It contains small rounded and totally micritized speleothem fragments that are 0.05 to 1 mm in size, and can be found "floating" in the groundmass. This microstructure alternates with the previous clast-supported microfacies in the upper part of the level (Fig. 6c, d).

Both microstructures display vesicular and vughy porosity that sometimes tends to be elongated in the vertical plane (Fig. 5).

4.1.3. Level G

Level G has a massive microstructure with a homogeneous groundmass consisting of reddish-brown sandy-silt sediment (RBS). The skeleton grains consist mainly of rounded and spherical allochthonous pebbles that are 0.3-1.0 cm in size, formed by sandstone and lutite lithoclasts, and opaque minerals, as well as a large number of bone fragments (0.2-3.4 mm), many with fractures occurring *in situ* (Fig. 7a, b). The groundmass is relatively homogeneous, with medium sand-size quartz grains and coarse silt (0.03-0.30 mm), as well as red clay. Some areas display clay-rich patches surrounded by a sandier matrix (Fig. 7c, d). Inside these clay-rich patches, there is an alternation between red clayey and siltier microfacies, showing possible original bedding of the sediments. Vertically elongated vesicular and vughy pores normally emerge from these fractured clay laminae patches (Figs. 7c, d). There are also a few fissure-type pores throughout the level.

4.1.4. Level F

Similar to the microfacies in level G, level F has a massive and fissure-type microstructure and homogeneous groundmass. The level consists of a sandy matrix with some vesicular and vughy porosity (Fig. 8). The skeleton grain is mainly comprised of very rounded and spherical allochthonous pebbles (0.3-1.0 cm) of sandstone and lutite lithoclasts, opaque minerals (Fig. 8) and 0.02-2.00 mm bone fragments (Fig. 8a). In the upper part of the level, one layer contains more anorthic ferruginous nodules, which slightly changes the ratio of skeleton grains to groundmass (Fig. 8b). The groundmass is relatively homogeneous with quartz grains from coarse silt to medium sand (0.03-0.30 mm), as well as silt and brown clay (BS) (Fig. 8). Remains of modern roots can be seen in some of the pores.

4.1.5. Level B

The microfacies in level B are practically the same as those described in level F, apart from the presence of calcite crystals. Level B has a massive microstructure with a homogeneous brown sandy-silt groundmass (BS). The skeleton grains consist of centimetric fragments of speleothems, very rounded and spherical allochthonous sandstone and lutite lithoclast and anorthic ferruginous pebbles that are 0.3-1.0 cm in size, and 0.2-0.5 mm bone fragments. The matrix is relatively homogeneous, with coarse silt to medium sand (0.03-0.30 mm) quartz grains embedded in brown and reddish clays (Fig. 9). There is also a 4 x 5 cm area cemented by sparitic calcite crystals, which enclose aggregates of different clastic cements, some similar to the matrix, others seen here for the first time, as well as some anorthic ferruginous nodules (Fig. 9).

4.2. X-Ray Diffraction (XRD) Mineralogy

The XRD results are given in Table 3. Due to the variety of clay-type microfacies differentiated in the micromorphological study, these mineralogical data have been re-evaluated and compared with the micromorphological study to determine whether or not they are complementary.

Bulk mineralogy data highlights that the calcite proportion in levels H and E is higher when compared to other levels. This is reasonable since one of the microstructures in level H was rich in flowstone fragments (Fig. 6), and level E appears cemented by the calcium-carbonate rich waters probably filtrated from the upper flowstone level D (Fig. 3). The rest of the levels show less variability in their mineralogy. Levels C and B display larger quantities of calcite than the rest of the levels (except E and H). Finally, level K has relatively higher proportion of feldspar.

The clay mineralogy in the levels studied exhibit different proportions of illite, vermiculite and some kaolinite. There is a noticeably high proportion of illitic clay in level K, as well as in levels I and E, which contrasts with the smaller amount of illite and increasing values of vermiculite found in levels H, G and B (Table 3). Arriolabengoa et al. (2015) established that vermiculite originates from the loss of potassium from illite. The origin of kaolinite clay mineral is more difficult to determine, since part of it can be inherited from the rocks, and some from the weathering of feldspar grains.

4.3. TT-OSL dating

The single-grain TT-OSL dating results are summarised in Table 4 and Fig. 10. ~3.7% of the individually measured grains were deemed suitable for D_e determination after applying the single-grain quality assurance criteria of Arnold et al. (2014). The D_e distribution (n=84 grains) is normally distributed according to the log skewness test outlined by Arnold and Roberts (2011). The D_e dataset is also characterised by relatively low overdispersion of 25 ± 5%, and the D_e scatter is well-represented by the weighted mean burial dose (as indicated by the large proportion of individual D_e values lying within the 2σ grey band in Fig. 10). These favourable D_e distribution characteristics are considered to reflect sufficient optical resetting of the accepted grain population prior to burial, and the absence of post-depositional sediment mixing (e.g., Bailey and Arnold, 2006; Arnold and Roberts, 2009; Arnold et al., 2013). The final burial dose has therefore been calculated using the central age model of Galbraith et al. (1999), and the resultant single-grain TT-OSL age for sample LZ12-6 is 215.7 ± 15.1 ka (1σ uncertainty range).

5. Discussion

5.1. Endokarstic Sedimentary Processes

The microfacies observed and described in the different stratigraphic units are the result of the interaction of diverse sedimentary and post-depositional processes. To determine these processes, and to understand their interactions and possible connection with environmental changes, it is necessary to characterise and interpret the sedimentary data and microstructures observed.

5.1.1. Calcite precipitation

Calcite precipitates have been found in levels I, H and B. However, their characteristics and interpretations vary in every level. In level I, the precipitates were only found locally filling the vesicular porosity at the top of the level, and the XRD analysis barely detected calcite (Table 3). The tabular and acicular crystal growth is perpendicular to the surface of the alveolar porosity (Fig. 4c) and is produced by the percolation of water saturated in carbonate, which precipitates in the pores, often assisted by roots (Hill and Forti, 1997; Karkanas and Goldberg, 2010). As the overlying Level H contains a large quantity of carbonate (Table 3), it is very likely that the carbonate-enriched water percolated and was later precipitated in the pore spaces of level I. This is therefore a post-depositional precipitation. In contrast, calcite in level H come from speleothem fragments (Figs. 5, 6). Fragments that still display structures marking the polarity of crystalline growth indicate that they have been redeposited (Fig. 6a) and have therefore not formed *in situ*. Even so, the fact that some fragments still preserve their original structure and are only slightly rounded shows that they were formed in close proximity and were not transported far. These calcite fragments probably formed through the circulation of a sheet of water (Ford and Williams, 2007), either in some inner part of the cave or coating the wall, and eroded or spalled when the sheet of water dried. The final example of calcite precipitation occurs in level B, where large sparite crystals agglutinate different types of lenticular micro-aggregates and anorthic ferruginous nodules (Fig. 9). Because of the rounded form of the cemented clast and the allochthonous micro-aggregates it contains, we believe that the level B calcite was not formed *in situ*, and is therefore considered to be a lithoclast.

5.1.2. Red and yellow clay matrix: source and transport mechanisms

The clays that form the different stratigraphic levels generally display a massive microstructure. Indeed, two main types of silty-clay matrixes were differentiated in this study, the reddish silty sediment (RsS) and the yellow sandy sediment (YSS) (Figs. 4a, 6b), which could be associated with both types of identified clastic sedimentary processes: infiltration and fluviokarstic processes (Arriolabengoa et al., 2015).

The groundmass in level H consists almost entirely of reddish silty-clay sediment (RsS) (Fig. 6), arranged massively (matrix-supported) and between speleothem fragments (clast-supported). RsS-type microfacies are characterised by the absence of allochthonous and coarse elements and good sorting of the massive red mud (aside from speleothem fragments) and correspond to low-energy sedimentary environments. The bedding in this level is provided by the intercalated speleothem fragments, while the RsS does not show any internal lamination. The lack of internal structure is a primary feature that occurs under the following possible scenarios: i) rapid deposition from suspension in the absence of traction transport (Boggs, 2012); ii) deposition from very highly concentrated sediments - hyperconcentrated flow - (Bertran and Texier, 1999); or iii) due to the stability of the sedimentary process (Valen et al., 1997). The mineralogical data show that the RsS from level H has the highest quantity of vermiculite (Table 3), a pedogenic clay mineral abundant in *terra rossa*-type soils formed on limestone substrates, corresponding to soil infiltration processes previously identified in this cave (Arriolabengoa et al., 2015). Infiltration of the upper soils into the cave could have occurred through diffuse drainage, which would have introduced the red silty-clay sediment into the cave, as well as produce the dripping along the gallery. The accumulation of the dripping water in the gallery can create small local pools in which RsS would deposit from suspension, and form these massive, homogeneous and fine-sediment deposits. In addition, diffuse drainage does regulate the recharge in caves, making the process relatively constant (Audra and Palmer, 2013) which would help in the formation of an absent bedding.

On the other hand, level H also displays small intrusions of a yellow sandy sediment (YSS) (Figs. 5, 6b) that has a different mineralogical composition, indicating a different source area and a higher energy transport process (Courty et al., 2012). In this regard, level I has the highest proportion of YSS but it is always poorly mixed with RsS (Fig. 4). Level I also contains rip-up clasts and millimetric size rounded lithoclasts in the skeleton (Fig. 4b), indicating erosion and resedimentation of other allochthonous deposits by higher energy processes, such as water flooding (Knapp et al., 2007). The mineralogical data show that the quantity of illite in level I is slightly lower than in level K (a fluviokarstic level), but higher than in the other stratigraphic levels (Table 3). A larger quantity of illite is characteristic of relatively young allochthonous soils formed on siliciclastic rocks in the valley (Arriolabengoa et al., 2015). It may, therefore, be concluded that the yellow sandy matrix (YSS) comes from the entry of allochthonous edaphic sediment through runoff or the entry of floodwater from a stream into the cave. The lack of bedding in those deposits could be related to hyperconcentration of the flow, which occurs in flood events if there is enough sediment available (Bertran and Texies, 1999).

Levels G, F and B are composed of a well-mixed RsS and YSS. level G also shows a reddish-brown silt and sand (BRS) groundmass while levels F and B show a brown sandy-silt (BS) groundmass; all of them display a massive homogeneous appearance and are poorly sorted (Figs. 7b, 8, 9). The clay mineralogy exhibits intermediate illite/vermiculite ratios compared to those in levels H and I. In level G, a primary intercalation of RsS and YSS layers can be observed forming a subtle lamination (Fig. 7c, d). At the same time this level contains higher vermiculite content than levels F and B (Table 3). Therefore, we deduce that level G displays alternating periods of relatively larger supply of sediment derived from percolation, rather than runoff. This alternation has led to the formation of bedding, which has been almost entirely destroyed by diagenetic processes. In contrast, level F does not contain rip-up clasts from other levels or patches of yellow sand; as such runoff, or river flooding, did not deposit allochthonous sediments during the formation of this level. However, anorthic ferruginous nodule grains are abundant in some parts of this level (Fig. 8). We therefore deduce that these deposits could have formed from inwash events, when part of the soil in the surroundings areas was eroded and transported into the cave through small entrances or shaft drains (Bosch and White, 2007). This type of process is more common during periods of low vegetation cover, when soil erosion is greater and materials can be remobilised (Courty and Vallverdu, 2001; Oliva-Urcia et al., 2014). The flow responsible for this could also have been hyperconcentrated in sediment, resulting in poor sorting of the microfabric (Courty and Vallverdu, 2001; Oliva-Urcia et al., 2014).

5.1.3. Post-depositional processes

In addition to the precipitation of secondary porosity-filling calcite in level I, other features also denote the action of post-depositional processes. In levels H and G, embedded in the red clay matrix (RsS), the vesicular and vughy porosity is sometimes elongated vertically (Figs. 6d, 7). This type of porosity forms when trapped air or water escapes due to pressure (van der Meer and Hiemstra, 1998; Phillips et al., 2007; Karkanas and Goldberg, 2013). Similarly, the fracturing of thin clay lamina in level G (Fig. 7c, d) are also interpreted as structures formed by porewater escape (Menzies et al., 2010; van der Meer and Menzies, 2011). In this interpretation, water was confined in the sand (YSS) layers and vesicular pores in the red clay (RsS) and escaped upwards by breaking the clay layers because of vertical compression. This post-depositional compression process is also observed in some microfauna bones from level G, which were broken *in situ*, indicating compression forces due to vertical loads (Fig. 7a, b). In cave dynamics, vertical pressure could be produced by roof collapse, however in Lezetxiki II this process has not been registered to occur with sufficient force. On the other hand, some studies have shown that broken-bone features can be formed due to trampling by large animals (e.g., Estévez et al., 2014). Taking into account that the upper level F is the richest level in *Ursus spelaeus* with 114 remains (Villaluenga et al., 2012), we assume that the vertical pressure was caused by the presence of those bears. Finally, evidence of dissolution and amorphous features of some bones (Fig. 4d) indicates that authigenic phosphates might have formed in level I (Karkanas et al., 1999).

5.2. Cave Chronology

Resolving the chronostratigraphy of Lezetxiki II has previously proved contentious because of difficulties in obtaining reliable and precise radiometric ages over the time range of interest, and because of potentially unclear assignments of paleontological remains to specific stratigraphic levels. Three radiometric ages have been published previously for Lezetxiki II cave: Falguères et al. (2005/2006) obtained an U/Th age of 74 ka for the flowstone corresponding to level D, after applying a correction for the high clay content of the speleothem, while Castaños et al. (2011) obtained amino acid racemisation (AAR) ages of 70.0 ka and 86.8 ka for two *Ursus* teeth from level J. As part of the present study, we have obtained a new TT-OSL age of 215 ± 15.1 ka for sediment from the upper part of level K.

Following reassessment of the available chronological data, we interpret the AAR ages obtained from level J to be potentially compromised on the grounds of methodological complications, poor consistency with surrounding ages, and weak correlation with faunal climatic interpretations. Our latest MIS 7 TT-OSL age for level K, together with the MIS 5/4 age obtained by Falguères et al. (2005/2006) for the flowstone located 1.5 m above Level J, suggest that the intervening AAR ages may be too young. The climatic associations and the relative age obtained from faunal remains from level J also show poor correspondence with the existing MIS 5 AAR ages. In particular, *Sicista betulina* (Rofes et al., 2012) found in level J is interpreted as a cold climate fauna, and its presence is more consistent with an MIS 6 age assignment, as inferred from the bracketing U/Th and TT-OSL ages. Additionally, the *Muscardinus* fossil found in level G is hypothetically linked to warm and humid conditions associated with an interstadial period of MIS 5 (Garcia-Ibaibarriaga et al., 2015), which would reinforce the apparent AAR age underestimation for the underlying level J. From a methodological perspective, the AAR ages may have been compromised by the choice of dating material or absence of a site-specific numerical calibration curve. Bones ultimately exhibit open system behaviour (Pike et al., 2002; Grün, 2006; Dobberstein et al., 2008), and numerical AAR ages obtained from such materials have been shown to be erroneous in comparable contexts (e.g., Rios-Garaizar et al., 2015b).

5.3. Sedimentary evolution and palaeoenvironmental insight

The Lezetxiki II cave is part of the upper cave level of the Bostiturrieta valley and was formed during an ancient stable base-level time interval (Expósito et al., 2015). The known sedimentary record of Lezetxiki II began to accumulate when the local phreatic level was still relatively close in height. The fluviokarstic deposits in level K belong to that initial phase. Taking into account that river incision rates in the Deba valley were ~0.08 mm/yr (Aranburu et al., 2015), and our latest TT-OSL study of the upper part of this level has yielded an age of 215 ± 15 ka (MIS 7), we can infer that the Bostiturrieta stream was more or less around 17.2 m above the current stream level. Probably the cave conduit was perched, but still the local phreatic level was close to the altitude of the floor of the cave (Fig. 11a). Level K also has an abundant microfauna assemblage with no evidence of reworking and/or transportation (García-Ibaibarriaga, 2012), suggesting that fluviokarstic processes were not continuous.

Level J was subsequently deposited and, although it contains some finer fluvial gravel, the relative percentage of vermiculite clay in this level is higher than in level K (Table 3), indicating a greater influence of infiltration from karstic soils (Fig. 11b). Therefore, the proportion of sediments derived from fluviokarst processes decreased while infiltration processes from autochthonous soils overlying the karst increased, probably due to the ongoing incision of the river.

The overlying level I attests to flowing water depositing allochthonous siliciclastic material into the karst system (pedosediments derived from siliciclastic soils in the valley) and the resedimentation of previous endokarstic deposits (Fig. 11c). The change from greater sedimentation by percolation in level J to the runoff processes in level I might be a consequence of climate cooling and/or reduced precipitation, which would have resulted in a diminished vegetation cover and subsequent soil erosion and redeposition by runoff into the cave (Goldberg and MacPhail, 2000; Courty and Vallverdu, 2001). As the River Bostiturrieta was cutting through the valley, it would have been unable to transport centimetric sized cobbles into the cave during flood events, as it did in level J, and only sand and silt was introduced, together with rip-up clasts. The transition from level I to H is erosive (Fig. 5), reflecting the high-energy nature of the water courses that entered the cave.

Level H was deposited onto the irregular upper contact of level I (Fig. 5). Level H thins out towards the entrance and eventually disappears. During sedimentation of level H, runoff stopped and red clay infiltration and speleothem formation predominated (Fig. 11d), as evidenced by a large sedimentary change. Eventually, relatively small pools of water formed in the cave resulting in the deposition of percolating vermiculite-rich RsS clay, while at times laminar sheets of water flowed and flowstone formed on nearby ground surfaces or cave walls. In the transition between the two processes, thin calcite flowstone clasts would have broken off and become resedimented on the quasi-horizontal surfaces, representing ancient cave floors (Fig. 5). During the onset of sedimentation in level H, high-energy water flows appear to have increased in frequency, depositing some sandy layers. In contrast, towards the top of the level, the sediment becomes finer, creating a matrix-supported deposit rather than clast-supported deposit (Figs. 6c, d). This might indicate a decrease in the intensity of water flows, likely in connection with thick vegetation cover and more developed soils that would retain surface runoff during relatively warm, wet periods (Li et al., 2011; Zhang et al., 2015). Both the formation of speleothems (Stoll et al., 2013; Moreno et al., 2013; Aranburu et al., 2015) and the development of soils and vegetation cover (Courty and Vallverdu, 2001; Bertran et al., 2008; Karkanas et al., 2008) would have been associated with relatively warmer and wetter periods. Because of the great change in sedimentary dynamics, from runoff processes to infiltration processes, we hypothesize that this might reflect the transition from a glacial stage MIS 6 (level I) to an interglacial stage MIS 5 (level H).

Level G thins out towards the inner part of the cave, where it finally disappears (Table 1, Fig. 3). Its base is defined by a sharp contact and the disappearance of speleothem fragments. It is mainly formed by inwash sedimentation of hyperconcentrated sediment flows (i.e., YSS) alternating with periods dominated by infiltration (i.e., RsS). Level G would have been a transitional level with sedimentary processes changing from relatively warm and wet conditions, in which infiltration of soil and speleothem growth predominated (level H), to a level formed by repeated inwash at the cave entrance (level F), associated with drier and colder periods. In any case, the presence of *Muscardinus avellanarius* in level G has been related to the warm, wet interstadial of MIS 5 (García-Ibaibarriaga et al., 2015). In addition, post-depositional microstructures caused by vertical compaction have been documented in both level G and level H. This vertical pressure was possibly created by the *Ursus spelaeus* that inhabited Lezetxiki II cave during the formation of level F (Villaluenga et al., 2012).

The transition between level G and F is gradual, as the red clay (RsS) content decreases slightly, supporting the hypothesis that level G is a transition level between two periods with different climates. During the formation of level F, inwash introduced sediment from the soils surrounding the cave (Fig. 11e). The flow energy was variable and, as a result, layers with coarser grain size have been found, consisting of a large amount of anorthic ferruginous nodule gravel (Fig. 8b). Therefore, the climate when level F was formed may have been cooler and drier than in previous levels, resulting in less dense vegetation cover and greater surface runoff, which would have eroded and redeposited soil sediment inside the cave (Courty and Vallverdú, 2011).

The grain size in level E is relatively coarse. However, this is not a primary feature, but is due to water percolation depositing the flowstone in level D and the formation of aggregates of cemented sediment. The flowstone in level D has been dated to 74 ka (Falguères et al., 2005/2006) and indicates the end of MIS 5 and the start of MIS 4.

The deposition of level C would have begun at the start of the relatively cold MIS 4-2 period (Stoll et al., 2013; Alvarez-Lao et al., 2015) (it contains Upper Palaeolithic archaeological remains). As the mineralogical traits of level C are very similar to those in level F (Table 3), it was probably also formed by sediment inwash into the cave. Additionally, one or several erosive processes (e.g., runoff) removed part of the endokarst sedimentary sequence in the area nearest to the cave entrance. These erosive events in endokarst sequences appear to be characteristic of colder and drier conditions predominating during the transition from interglacial to glacial periods (Aranburu et al., 2015).

Level B, based on its Chalcolithic archaeological assemblage (Table 1), was deposited during MIS 1 on top of the aforementioned erosional surface. The surface between the two levels is almost imperceptible at a microscopic scale, as inwash processes produced sedimentation in both units.

6. Conclusions

Micromorphological analysis of the sedimentary record at Lezetxiki II, aided by XRD data, has enabled us to reveal correlations between paleoenvironmental changes and sedimentary processes in this cave, which started during MIS 7 (level K). A considerable sedimentary change is identified from level I to level H, where runoff processes that carry allochthonous sediment were replaced abruptly by low energy infiltration processes carrying autochthonous upper soils into the cave. We interpret this variation as reflecting abrupt climatic change, hypothetically associated with the MIS 6-MIS 5e transition. The remaining variations in microfacies were not as abrupt as from levels I to H. The changes from infiltration to inwash processes in level F, and their intensity, are interpreted as corresponding to the MIS 5 interestadial / stadial oscillations. Finally, level B showed practically the same microstructure and microfacie as level F, suggesting that during the main parts of these interglacial periods (i.e., MIS 5 and MIS 1) inwash processes were the most common occurrences at this site. In a general sense, the microstratigraphic changes registered in this work are consistent with other sedimentary records obtained from speleothem growth (Stoll et al., 2013) and cave stratigraphy studies from the Cantabrian Margin (Aranburu et al., 2015), and help to further connect local and regional paleoenvironmental oscillations with global climatic changes.

The Lezetxiki archaeological complex contains a sedimentary record that is at least 215 ± 15.1 ka, and is currently one of the oldest prehistoric human sites in the northern Iberian Peninsula. The archaeological and paleontological remains at Lezetxiki II have not suffered severe diagenetic processes, and show limited instance of breakage and alterations in microfaunal bones. The data obtained in this work provide an overview of the sedimentary processes affecting the Lezetxiki cave environment and allow microstratigraphic correlations with the rest of the excavations. As such, this study represents the first step towards reconstructing the broader sedimentary history of the Lezetxiki archaeological complex. The application of similar micromorphological studies at other sites of the Cantabrian Margin should help to broaden our knowledge of how related sedimentary systems responded to regional paleoenvironmental changes, as well establishing firmer paleoenvironmental frameworks for understanding prehistoric human occupation patterns across the region.

Acknowledgements

The authors would like to acknowledge the PALEOGATE project, funded by the Spanish Ministry of Economy and Competitiveness (HAR2014-53536-P) as well as the US14/16 project funded by the University of the Basque Country and Basque Coast Geopark, and Basque Government (IT1029-16-GBV6). We would also like to thank Tim Nicholson for his work in translating and editing different versions of the English text. Additional financial support for this research was provided by Australian Research

Council (ARC) Future Fellowship project FT130100195, ARC Discovery Early Career Researcher Award DE160100743. L.A. and M.D. thank Carlos Pérez Garrido for his assistance with preparing and measuring the luminescence dating samples at the CENIEH luminescence dating laboratory, Burgos, Spain. We thank Dr. Daniel Ballesteros, Dr. Jasper Knight and an anonymous reviewer for constructive comments that enhanced the quality of the article.

References

Altuna, J., 1972. Fauna de mamíferos de los yacimientos prehistóricos de Guipúzcoa. Con Catálogo de los Mamíferos Cuaternarios del Cantábrico y del Pirineo Occidental. Munibe 24, 14-64.

Álvarez-Alonso, D., 2014. First Neanderthal settlements in northern Iberia: The Acheulean and the emergence of Mousterian technology in the Cantabrian region. Quaternary International 326-327, 288-306.

Álvarez-Lao, D.J., Ruiz-Zapata, M., Gil-García, M., Ballesteros, D., Jiménez-Sánchez, M., 2015. Palaeoenvironmental research at Rexidora Cave: new evidence of cold and dry conditions in NW Iberia during MIS 3. Quaternary International 379, 35-46.

Aranburu, A., Arriolabengoa, M., Iriarte, E., Giralt, S., Yusta, I., Martínez-Pillado, V., del Val, M., Moreno, J., Jiménez-Sánchez, M., 2015. Karst landscape evolution in the littoral area of the Bay of Biscay (north Iberian Peninsula). Quaternary International 364, 217–230.

Arnold, L.J., Roberts, R.G., 2009. Stochastic modelling of multi-grain equivalent dose (D_e) distributions: Implications for OSL dating of sediment mixtures. Quaternary Geochronology 4, 204–230.

Arnold, L.J., Roberts, R.G., 2011. Paper I - optically stimulated luminescence (OSL) dating of perennially frozen deposits in north-central Siberia: OSL characteristics of quartz grains and methodological considerations regarding their suitability for dating. Boreas 40, 389-416.

Arnold, L.J., Demuro, M., 2015. Insights into TT-OSL signal stability from single-grain analyses of known-age deposits at Atapuerca, Spain. Quaternary Geochronology 30, 472-478.

Arnold, L.J., Demuro, M., Navazo Ruiz, M., Benito-Calvo, A., Pérez-González, A., 2013. OSL dating of the Middle Palaeolithic Hotel California site, Sierra de Atapuerca, north-central Spain. Boreas 42, 285-305.

Arnold, L.J., Demuro, M., Parés, J.M., Arsuaga, J.L., Aranburu, A., Bermúdez de Castro, J.M., Carbonell, E., 2014. Luminescence dating and palaeomagnetic age constraint on hominins from Sima de los Huesos, Atapuerca, Spain. Journal of Human Evolution 67, 85-107.

Arnold, L.J., Demuro, M., Parés, J.M., Pérez-González, A., Arsuaga, J.L., Bermúdez de Castro, J.M., Carbonell, E., 2015. Evaluating the suitability of extended-range luminescence dating techniques over Early and Middle Pleistocene timescales: Published datasets and case studies from Atapuerca, Spain. Quaternary International 389, 167-190.

Arnold, L.J., Duval, M., Falguères, C., Bahain, J.-J., Demuro, M., 2012. Portable gamma spectrometry with cerium-doped lanthanum bromide scintillators: Suitability assessments for luminescence and electron spin resonance dating applications. Radiation Measurements 47, 6–18.

Arostegui, J., Sangüesa, F.J., Nieto, F., Uriarte, J.A., 2006. Thermal models and clay diagenesis in the Tertiary-Cretaceous sediments of the Alava block (Basque-Cantabrian basin, Spain). Clay Minerals 41, 791-806.

Arriolabengoa, M., Iriarte, E., Aranburu, A., Yusta, I., Arrizabalaga, A., 2015. Provenance study of endokarst fine sediments through mineralogical and geochemical data (Lezetxiki II cave, northern Iberia). Quaternary International 364, 231–243.

Arrizabalaga, A., 2006. Lezetxiki (Arrasate, País Vasco). Nuevas preguntas acerca de un antiguo yacimiento. In: Cabrera, V., Bernaldo de Quiros, F., Maillo, J.M. (Eds.), Centenario de la Cueva de El Castillo: el ocaso de los Neandertales. UNED, Santander, pp. 291-310.

Arrizabalaga, A., Altuna, J., Areso, P., Falgueres, C., Iriarte, M.J., Mariezkurrena, K., Pemán, E., Ruíz-Alonso, M., Tarriño, A., Uriz, A., Vallverdú, J., 2004. Retorno a Lezetxiki (Arrasate, País Vasco): nuevas perspectivas de la investigación. In: Santoja, M., Pérez-González, A., Machado, M.J. (Eds.), Geoarqueología y Conservación del Patrimonio. ADEMA, Almazán, pp. 63-80.

Arrizabalaga, A., Rios-Garaizar, J., 2012. The first human occupation of the Basque Crossroads. Journal of World Prehistory 25, 157-181.

Arrizabalaga, A., Ríos-Garaizar, J., Maíllo-Fernández, J.M., Iriarte-Chiapusso, M.J., 2014. Identifying the Signs: The Middle to Upper Palaeolithic Transition in northern iberia from the Perspective of the Lithic Record. Journal of Lithic Studies 1, 151-166.

Audra, P., Palmer, A.N., 2013. The vertical dimension of karst: controls of vertical cave pattern. In: Shroder, J.F. (Ed.), Treatise on Geomorphology, Vol. 6. Elsevier, San Diego, pp. 186-206.

Bailey, R.M., Arnold, L.J., 2006. Statistical modelling of single grain quartz De distributions and an assessment of procedures for estimating burial dose. Quaternary Science Reviews 25, 2475-2502.

Ballesteros, D., Jiménez-Sánchez, M., Giralt, S., DeFelipe, I., García-Sansegundo, J., 2017. Glacial origin for cave rhythmite during MIS 5d-c in a glaciokarst landscape, Picos de Europa (Spain). Geomorphology 286, 68-77.

Barandiarán, J.M., Altuna, J., 1970. Excavación de la cueva de Lezetxiki (Campaña de 1968). Munibe 22, 51-59.

Basabe, J.M., 1966. El húmero premusteriense de Lezetxiki (Guipúzcoa). Munibe 1/4, 13-32.

Benyarku, C.A., Stoops, G., 2005. Guidelines for Preparation of Rock and Soil Thin Sections and Polished Sections. Department of Environment and Soil Science, University of Lleida. Lleida, 84 pp.

Bertran, P., Caner, L., Langohr, R., Lemée, L., d'Errico, F., 2008. Continental palaeoenvironments during MIS 2 and 3 in southwestern France: the La Ferrassie rockshelter record. Quaternary Science Reviews 27, 2048–2063.

Bertran, P., Texier, J.P., 1999. Facies and microfacies of slope deposits. Catena 35, 99–121.

Boggs, S. Jr., 2012. Principles of sedimentology and stratigraphy. Pearson Prentice Hall, New Jersey, 585 pp.

Bosch, R.F., White, W.B., 2004. Lithofacies and transport of clastic sediments in karstic aquifers. In: Sasowsky, I.D., Mylroie, J. (Eds), Studies of Cave Sediments: Physical and Chemical Records of Paleoclimate. Springer, New York, pp. 95-106.

Bowler, J.M., Johnston, H., Olley, J.M., Prescott, J.R., Roberts, R.G., Shawcross, W., Spooner, N.A., 2003. New ages for human occupation and climatic change at Lake Mungo, Australia. Nature 421, 837-840.

Brennan, B.J., 2003. Beta doses to spherical grains. Radiation Measurements 37, 299–303.

Bull, P.A., 1981. Some fine-grained sedimentation phenomena in caves. Earth Surface Processes and Landforms 6, 11–22.

Bullock, P., Fédoroff, N., Jongerius, A., Stoops, G., Tursina, T., 1985. Handbook for Soil Thin Section Description. Waine Rersearch Publications, Albrighton, 152 pp.

Canti, M., Huisman, D.J., 2015. Scientific advances in geoarchaeology during the last twenty years. Journal of Archaeological Science 56, 96–108.

Castaños, P., Murelaga, X., Arrizabalaga, A., Iriarte, M.J., 2011. First evidence of Macaca sylvanus (Primates, Cercopithecidae) from the Late Pleistocene of Lezetxiki II cave (Basque Country, Spain). Journal of Human Hvolution 60, 816–20.

Courty, M.A., Vallverdu, J., 2001. The Microstratigraphic Record of Abrupt Climate Changes in Cave Sediments of the Western Mediterranean. Geoarchaeology - An International Journal 16, 467–500.

Courty, M.A., Carbonell, E., Vallverdú, J., Banerjee, R., 2012. Microstratigraphic and multi-analytical evidence for advanced Neanderthal pyrotechnology at Abric Romani (Capellades, Spain). Quaternary International 247, 294–312.

Demuro, M., Arnold, L.J., Parés, J.M., Pérez-González, A., Ortega, A.I., Arsuaga, J.L., Bermúdez de Castro, J.M., Carbonell, E., 2014. New luminescence ages for the

Galería Complex archaeological site: Resolving chronological uncertainties on the Acheulean record of the Sierra de Atapuerca, northern Spain. PLoS ONE 9, e110169, doi: 10.1371/journal.pone.0110169.

Demuro, M., Arnold, L.J., Parés, J.M., Sala, R., 2015. Extended-range luminescence chronologies suggest potentially complex bone accumulation histories at the Early-to-Middle Pleistocene palaeontological site of Huéscar-1 (Guadix-Baza basin, Spain). Quaternary International 389, 191-212.

Dobberstein, R.C., Huppertz, J., von Wurmb-Schwark, N., Ritz-Timme, S., 2008. Degradation of biomolecules in artificially and naturally aged teeth: Implications for age estimation based on aspartic acid racemization and DNA analysis. Forensic Science International 179, 181-191.

Estévez, J., Villagran, X.S., Balbo, A.L., Hardy, K., 2014. Microtaphonomy in archaeological sites: The use of soil micromorphology to better understand bone taphonomy in archaeological contexts. Quaternary International 330, 3–9.

Expósito, J.M., Arriolabengoa, M., Azkoaga, X., Dorado, J., Zabaleta, P., Berezibar, A., Esperasate, J.L., Abarrategi, B., Eraña, C., Ugarte, S., Pereda, L., Richard, L., Olalde, A., 2015. Desarrollo de niveles kársticos en el valle del Bostiturrieta (Arrasate). Karaitza 23, 14-23.

EVE., 1992. Mapa Geológico del País Vasco a escala 1:25.000, Hoja Otxandio 87-IV. Energiaren Euskal Erakundea/Ente Vasco de Energía.

Falguères, C., Yokoyama, Y., Arrizabalaga, A., 2005/2006. La geocronología del yacimiento pleistocénico de Lezetxiki (Arrasate, País Vasco). Crítica de las dataciones existentes y algunas nuevas aportaciones. Munibe 52/2, 93-106.

Fairchild, I.J., Baker, A., 2012. Speleothem Science: From Process to Past Environments. Wiley-Blackwell, Chichester, 432 pp.

Ford, D., Williams, P., 2007. Karst Hydrogeology and Geomorphology. John Wiley & Sons, Chichester, 578 pp.

Galbraith, R.F., Roberts, R.G., Laslett, G.M., Yoshida, H., Olley, J.M. 1999. Optical dating of single and multiple grains of quartz from Jinmium rock shelter, northern Australia: Part I. Experimental design and statistical models. Archaeometry 41, 339–364.

García-Ibaibarriaga, N., 2012. El registro de micromamíferos del nivel basal de Lezetxiki II (Arrasate, País Vasco). CKQ Quaternary Studies 1, 71-84.

Garcia-Ibaibarriaga, N., Arrizabalaga, A., Iriarte-Chiapusso, M.J., Rofes, J., Murelaga, X., 2015. The return to the Iberian Peninsula: first Quaternary record of Muscardinus and a palaeogeographical overview of the genus in Europe. Quaternary Science Reviews 119, 106–115.

García-Mondéjar, J., 1990. The Aptian-Albian carbonate episode of the Basque-Cantabrian basin (northern Spain): general characteristics, controls and evolution. In: Tucker, M.E., Wilson, J.L., Crevello, P.D., Sarg, J.F., Read, J.F. (Eds.), Carbonate Platforms: Facies, Sequences and Evolution. IAS Special Publications 9, Blackwell, Oxford, pp. 257-290.

Gázquez, F., Calaforra, J.M., Forti, P., Stoll, H., Ghaleb, B., Delgado-Huertas, A., 2014. Paleoflood events recorded by speleothems in caves. Earth Surface Processes and Landforms 39, 1345-1353.

Goldberg, P., MacPhail, R., 2000. Micromorphology of sediments from Gibraltar caves: some preliminary results from Gorham's cave and Vanguard Cave. In: Finlayson, J.C., Finlayson, G., Fa, D.A. (Eds.), Gibraltar during the Quaternary. Gibraltar Government Herigate Publication Monographs 1, pp. 93–108.

Gómez-Olivencia, A., Arceredillo, D., Álvarez-lao, D.J., Garate, D., San Pedro, Z., Castaños, P., Rios-Garaizar, J., 2014. New evidence for the presence of reindeer (Rangifer tarandus) on the Iberian peninsula in the Pleistocene: an archaeopalaeontological and chronological reassessment. Boreas 43, 286-308.

González-Lemos, S., Müller, W., Pisonero, J., Cheng, H., Edwards, R.L., Stoll, H.M., 2015a. Holocene flood frequency reconstruction from speleothems in northern Spain. Quaternary Science Reviews 127, 129-140.

González-Lemos, S., Jiménez-Sánchez, M., Stoll, H.M., 2015b. Sediment transport during recent cave flooding events and characterization of speleothem archives of past flooding. Geomorphology 228, 87-100.

Grün, R, 2006. Direct dating of human fossils. American Journal of Physical Anthropology 131, 2-48.

Guérin, G., Mercier, M., Adamiec, G., 2011. Dose-rate conversion factors. update. Ancient TL 29, 5–8.

Hill, C., Forti, P., 1997. Cave Minerals of the World. National Speleological Society, Huntsville AL, 433 pp.

Inglis, R.H., French, C., Farr, L., Hunt, C.O., Jones, S.C., Reynolds, T., Baker, G., 2016. Sediment micromorphology and site formation processes during the Middle to Later Stone Ages at the Haua Fteah Cave, Cyrenaica, Libya. Geoarchaeology 33, 328-348.

Karkanas, P., Goldberg, P., 2010. Site formation processes at Pinnacle Point Cave 13B (Mossel Bay, Western Cape Province, South Africa): resolving stratigraphic and depositional complexities with micromorphology. Journal of Human Evolution 59, 256–273.

Karkanas, P., Goldberg P., 2013. Micromorphology of Cave Sediments. In: Shroder J.F. (Ed.), Treatise on Geomorphology, Vol. 6. Elsevier, San Diego, pp. 286–297.

Karkanas, P., Kyparissi-Apostolika, N., Bar-Yosef, O., Weiner, S., 1999. Mineral Assemblages in Theopetra, Greece: A Framework for Understanding Diagenesis in a Prehistoric Cave. Journal of Archaeological Science 26, 1171–1180.

Karkanas, P., Bar-Yosef, O., Goldberg, P., Weiner, S., 2000. Diagenesis in Prehistoric Caves: the Use of Minerals that Form In Situ to Assess the Completeness of the Archaeological Record. Journal of Archaeological Science 27, 915–929.

Karkanas, P., Schepartz, L.A., Miller-Antonio, S., Wang, W., Huang, W., 2008. Late Middle Pleistocene climate in southwestern China: inferences from the stratigraphic record of Panxian Dadong Cave, Guizhou. Quaternary Science Reviews 27, 1555–1570.

Knapp, E., Mahler, B.J., Hauwert, N.N., 2004. Readign Virginia´s Paleoclimate from the geochemistry and sedimentology of clastic cave sediments. In: Sasowsky, I.D., Mylroie, J. (Eds), Studies of Cave Sediments: Physical and Chemical Records of Paleoclimate. Springer, New York, pp. 95-106.

Li, X.Y., Contreras, S., Solé-Benet, A., Cantón, Y., Domingo, F., Lázaro, R., Lin, H., Wesemael, B.V., Puigdefábregas, J., 2011. Controls of infiltration-runoff processes in Mediterranean karst rangelands in SE Spain. Catena 86, 98-109.

Mallol, C., Cabanes, D., Baena, J., 2010. Microstratigraphy and diagenesis at the upper Pleistocene site of Esquilleu Cave (Cantabria, Spain). Quaternary International 214, 70-81.

Mejdahl, V., 1979. Thermoluminescence dating: beta-dose attenuation in quartz grains. Archaeometry 21, 61–72.

Menzies, J., van der Meer, J.J.M., Domack, E., Wellner, J.S., 2010. Micromorphology: as a tool in the detection, analyses and interpretation of (glacial) sediments and man-made materials. Proceedings of the Geologists' Association 121, 281–292.

Moreno, A., Belmonte, A., Bartolomé, M., Sancho, C., Oliva, B., Stoll, H., Edwards, L.R., Cheng, H., Hellstrom, J., 2013. Formación de espeleotemas en el noreste peninsular y su relación con las condiciones climáticas durante los últimos ciclos glaciares. Cuadernos de Investigación Geográfica 39, 25-47.

Morley, M.W., Goldberg, P., Sutikna, T., Tocheri, M.W., Prinsloo, L., Jatmiko, Saptomo, E.W., Wasisto, S., Roberts, R.G., 2017. Initial micromorphological results from Liang Bua, Flores (Indonesia): Site formation processes and hominin activities at the type locality of *Homo floresiensis*. Journal of Archaeological Science 77, 125-142.

Nejman, L., Lisá, L., Doláková, N., Horácek, I., Bajer, A., Novák, J., Wright, D., Sullivan, M., Wood, R., Gargett, R.H., Pacher, M., Sázelová, S., Nývltová Fisáková M., Rohovec, J., Králik, M., 2018. Cave deposits as a sedimentary trap for the Marine Isotope Stage 3 environmental record: The case study of Pod Hradem, Czech Republic. Palaeogeography, Palaeoclimatology, Palaeoecology 497, 201-217.

Nichols, G., 2009. Sedimentology and stratigraphy. Wiley-Blackwell, Chichester, 419 pp.

Oliva-Urcia, B., Bartolomé, M., Moreno, A., Gil-Romera, G., Sancho, C., Muñoz, A., Osácar, M.C., 2014. Testing the reliability of detrital cave sediments as recorders of paleomagnetic secular variations, Seso Cave System (Central Pyrenees, Spain). Catena 119, 36–51.

Phillips, E., Merritt, J., Auton, C., Golledge, N., 2007. Microstructures in subglacial and proglacial sediments: understanding faults, folds and fabrics, and the influence of water on the style of deformation. Quaternary Science Reviews 26, 1499–1528.

Pike, A.W.G., Hedges, R.E.M., van Calsteren, P., 2002. U-series dating of bone using the diffusion-adsorption model. Geochimica et Cosmochimica Acta 66, 4273-4286.

Prescott, J.R., Hutton, J.T., 1994. Cosmic ray contributions to dose rates for luminescence and ESR dating: large depths and long-term time variations. Radiation Measurements 23, 497–500.

Reading, H.G., 1996. Sedimentary Environments: Processes, Facies and Stratigraphy. Wiley-Blackwell, Cambridge, 704 pp.

Reineck, H.E., Singh, I.B., 1980. Depositional Sedimentary Environments. Springer-Verlag, Berlin, 550 pp.

Rios-Garaizar, J., Eixea, A., Villaverde, V., 2015a. Ramification of lithic production and the search of small tools in iberian Peninsula Middle Paleolithic. Quaternary International 361, 188-199.

Rios-Garaizar, J., Garate, D., Gómez-Olivencia, A., Iriarte, E., Arceredillo-Alonso, D., Iriarte-Chiapusso, M.J., García-Ibaibarriaga, N., García-Moreno, A., Gutierrez-Zugasti, I., Torres, T., Aranburu, A., Arriolabengoa, M., Bailón, S., Murelaga, X., Ordiales, A., Ortiz, J.E., Rofes, J., San Pedro, Z., 2015b. Short-term Neandertal occupations in the late Middle Pleistocene of Arlanpe (Lemoa, northern Iberian Peninsula). Comptes rendus - Palevol 14, 233-244.

Rofes, J., García-Ibaibarriaga, N., Murelaga, X., Arrizabalaga, A., Iriarte, M.J., Cuenca-Bescós, G., Villaluenga, A., 2012. The southwesternmost record of Sicista (Mammalia; Dipodidae) in Eurasia, with a review of the palaeogeography and palaeoecology of the genus in Europe. Palaeogeography, Palaeoclimatology, Palaeoecology 348-349, 67–73.

Sasowsky, I.D., Mylroie J., 2004. Studies of cave sediments: physical and chemical records of paleoclimate. New York, Springer, 328 pp.

Stephens, M., Rose, J., Gilbertson, D.D., 2017. Post-depositional alteration of humid tropical cae sediments: Micromorphological research in the Great Cave of iah, Sarawak, Borneo. Journal of Archaeological Science 77, 109-124.

Stoll, H.M., Moreno, A., Mendez-Vicente, A., Gonzalez-Lemos, S., Jimenez-Sanchez, M., Dominguez-Cuesta, M.J., Edwards, R.L., Cheng, H., Wang, X. 2013. Paleoclimate and growth rates of speleothems in the northwestern Iberian Peninsula over the last two glacial cycles. Quaternary Research 80, 284–290.

Stoops, G.J., 2003. Guidelines for analysis and Description of soil and Regolith Thin Sections. Soil Science Society of America, Madison, 184 pp.

Turk, J., 2011. Geoarchaeological research into Palaeolithic cave sites as a source of palaeoenvironmental data. Arheoloski Vestnik 62, 9–31.

Valen, V., Lauritzen, S.E., Lovlie, R., 1997. Sedimentation in a high-latitude karst cave: Sirijordgrotta, Nordland, Norway. Norsk Geologisk Tidsskrift 77, 233-250.

van der Meer, J.J.M., Hiemstra, J.F., 1998. Micromorphology of Miocene Diamicts, Indications of Grounded Ice. Terra Antartica 5, 363–366.

van der Meer, J.J.M., Menzies, J., 2011. The micromorphology of unconsolidated sediments. Sedimentary Geology 238, 213–232.

Velde, B., Meunier, A., 2008. The Origin of Clay Minerals in Soils and Weathering Rocks. Springer, Berlin, 351 pp.

Villaluenga, A., Monrepos, S., Castaños, P., Antonio, J., Alustiza, M., 2012. Cave Bear (*Ursus spelaeus* Rosenmüller Heinroth, 1794) and Humans During the Early Upper

Pleistocene (Lower and Middle Palaeolithic) in Lezetxiki , Lezetxiki II and Astigarragako Kobea. Journal of Taphonomy 10, 521–543.

Ward, I., Veth, P., Prossor, L., Denham, T., Ditchfield, K., Manne, T., Kendrick, P., Byrne, C., Hook, F., Troitzsch, U., 2017. 50.000 years of archaeological site stratigraphy and micromorphology in Boodie Cave, Barrow Island, Western Australia. Journal of Archaeological Science: Reports 15, 344-369.

White, W.B., 2007. Cave sediments and paleoclimate. Journal of Cave and Karst Studies 69, 76–93.

Zhang, L., Wang, J., Bai, Z., Lv, C., 2015. Effects of vegetation on runoff and soil erosion on reclaimed land in an opencast coal-mine dump in a loess area. Catena 128, 44-53.

Figure captions

Fig. 1. (a) Iberian Peninsula, Cantabrian Margin and the location of the study area; (b) types of soil along the Bostiturrieta valley. The limit between S2 and S3 is extrapolated from a limited number of outcrops and is subject to change.

Fig. 2. (a) Position of the Lezetxiki archaeological complex and Lezetxiki II cave in the Bostiturrieta valley (modified from Expósito et al., 2015); (b) General view of the Lezetxiki archaeological site; (c) View from the Arrizabalaga excavation trench toward the Barandiaran excavation. Dashed line represents the limits of the Barandiaran excavation trench, while the diagonal lines at the background of the image represent the excavated profile; (d) Plan view of the Lezetxiki archaeological complex excavation trenches and Lezetxiki II cave location.

Fig. 3. Stratigraphic column and profile of the sedimentary sequence of Lezetxiki II cave (modified from Arriolabengoa et al., 2015), showing the location of the samples taken for micromorphological, X-ray diffraction and TT-OSL analysis. Levels A-K are described in Table 1.

Fig. 4. Microphotographs of level I: (a) Mixing of reddish silty sediment (RsS) and yellow sandy sediment (YSS), giving the level a heterogeneous aspect; (b) Rip-up clasts aggregates (A); (c) Vughy porosity filled with acicular crystals of $CaCO_3$ (C); (d) Fragments of bone (B) and altered bone (AB).

Fig. 5. Microstructure and microfacies of the lower part of Level H, showing the irregular boundary between Levels I and H. The position of the speleothem fragments according to the direction of crystalline growth, and intercalations of yellow sandy sediment (YSS) sediment.

Fig. 6. Microphotographs of level H: (a) Inverted speleothem fragment (S, the arrow shows the direction of crystal growth), embedded in RsS; (b) Intercalation of different sediment types (RsS and YSS), under cross-polarised light (XPL); (c) Alternation of the reddish clay microstructure (matrix support - MS) and the speleothem-fragment-supported microstructure (Clast support - CS); (d) RsS microfacies with many vesicular and vughy pores (V), under XPL.

Fig. 7. Microphotographs of level G. (a) and (b) *In situ* broken bone fragments (B), embedded in reddish-brown sandy silt sediment (RBS); (c) Clay-rich patches (P) areas surrounded by sandy matrix and vertically elongated pores (V), which have been interpreted as porewater escape structures. Blue arrows represent the water movement; (d) Detail of 6c microphotograph, showing the intercalation between red clayey and fine-sandy microfacies inside the clay-rich patches, representing the original bedding (OB).

Fig. 8. Microphotographs of level F. (a) Microvertebrate tooth fragment (T) embedded in brown sandy silt sediment (BS); (b) Anorthic ferruginous nodules (N) rich layer with vesicular and vughy pores (V); (c) vesicular voids (V) and sandstone clast (S) embedded in BS; (d) same as (c) under XPL.

Fig. 9. Microphotographs of Level B. (a) The area cemented by sparitic calcite crystals (S) embedding aggregates (A) of different composition, as well as some anorthic ferruginous nodules (N). Outside the cemented area, there is brown sandy sediment (BS); (b) detail of the previous photograph; (c) same as 8b under XPL; (d) BS microfacies with some modern root remains (R).

Fig. 10. Single-grain TT-OSL equivalent dose (D_e) distribution for sample LZ12-6, shown as a radial plot.

Fig. 11. Schematic evolution of sedimentary fill in Lezetxiki II cave and proposed evolution of depositional processes and environmental conditions. Red coloured soils represent a well-developed soil, while the yellow coloured soil represents a less developed soil. Colours of cave sediments are given representing each stratigraphic level used in Fig. 3.

Table captions:

Table 1. Main features of the stratigraphic levels in Lezetxiki II cave and their archaeological and paleontological content (modified from Arriolabengoa et al., 2015).

Table 2. Main micromorphological characteristics of the stratigraphic levels in Lezetxiki II cave.

Table 3. Semi-quantitative (%) XRD analysis of endokarstic sediment samples from Lezetxiki II cave (modified from Arriolabengoa et al., 2015). Mineral abbreviations: Qtz: quartz, Cal: calcite, CM: phyllosilicates (mainly as clay minerals), Fsp: feldspar, Hap: hydroxylapatite, Gt: goethite, Vrm: vermiculite, Ill: illite, Kln: kaolinite.

Table 4. TT-OSL dose rate data, single-grain equivalent dose and final age for sample LZ12-6. The final TT-OSL age has been derived by dividing the weighted mean equivalent dose (D_e) by the total dose rate.

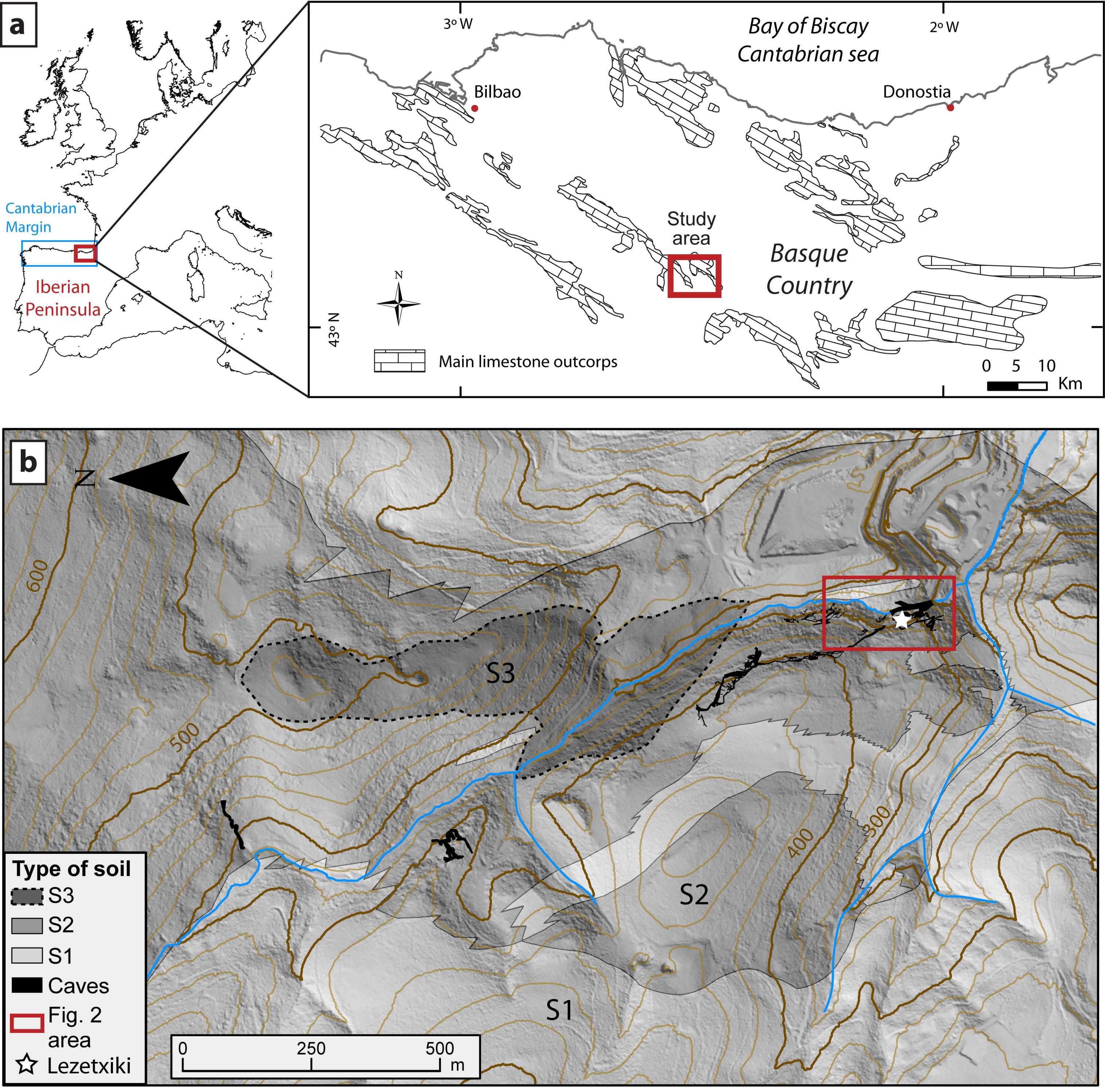
a
Cantabrian Margin
Iberian Peninsula
3° W
2° W
Bay of Biscay
Cantabrian sea
Bilbao
Donostia
Study area
Basque Country
N
43° N
Main limestone outcorps
0 5 10
Km
b
N
600
500
400
300
S3
S2
S1
Type of soil
S3
S2
S1
Caves
Fig. 2 area
Lezetxiki
0 250 500
m

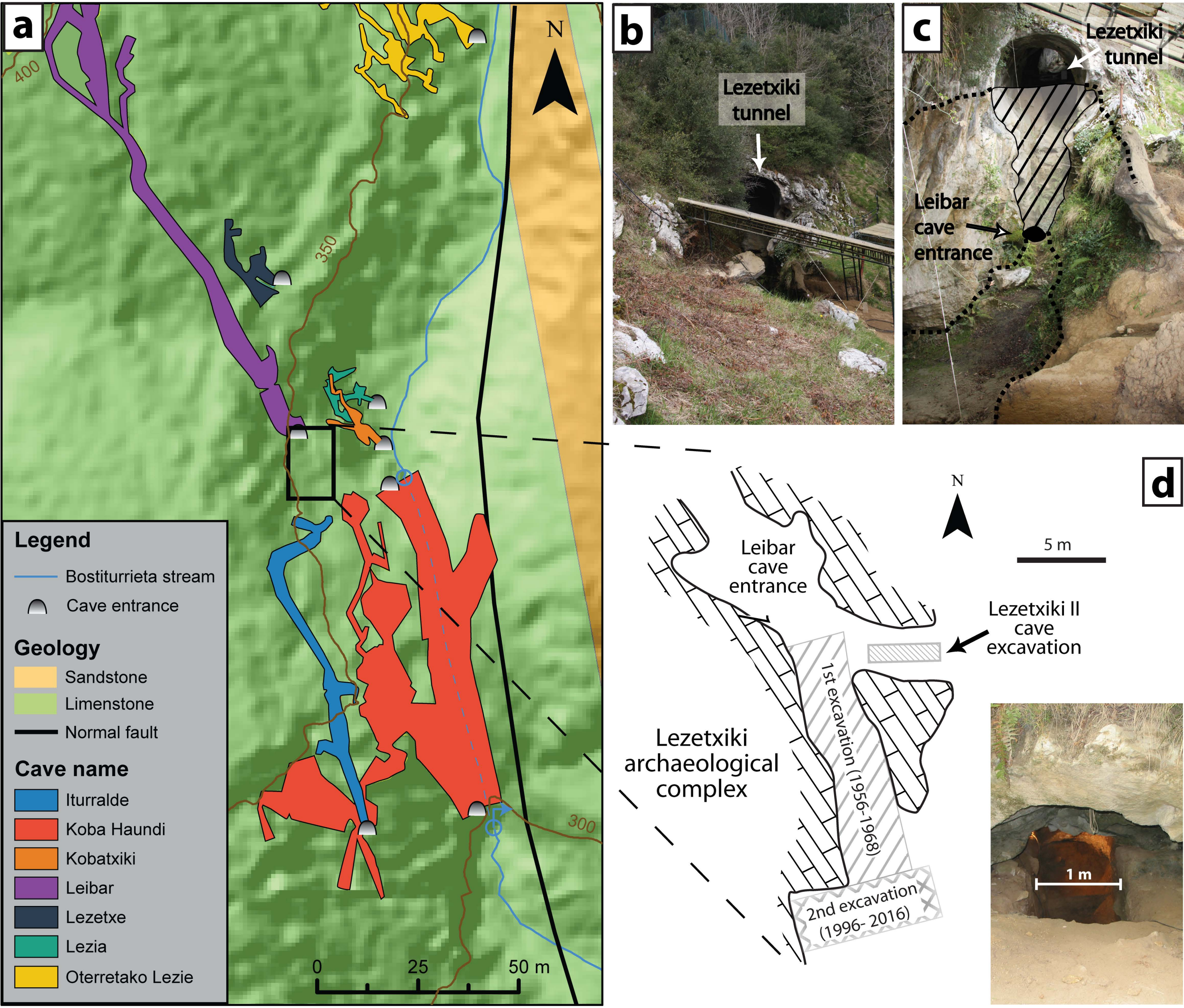

a
b
c
d
N
400
350
300
Legend
Bostiturrieta stream
Cave entrance
Geology
Sandstone
Limenstone
Normal fault
Cave name
Iturralde
Koba Haundi
Kobatxiki
Leibar
Lezetxe
Lezia
Oterretako Lezie
0
25
50 m
Lezetxiki tunnel
Leibar cave entrance
5 m
Leibar cave entrance
Lezetxiki II cave excavation
1st excavation (1956-1968)
2nd excavation (1996- 2016)
Lezetxiki archaeological complex
1 m

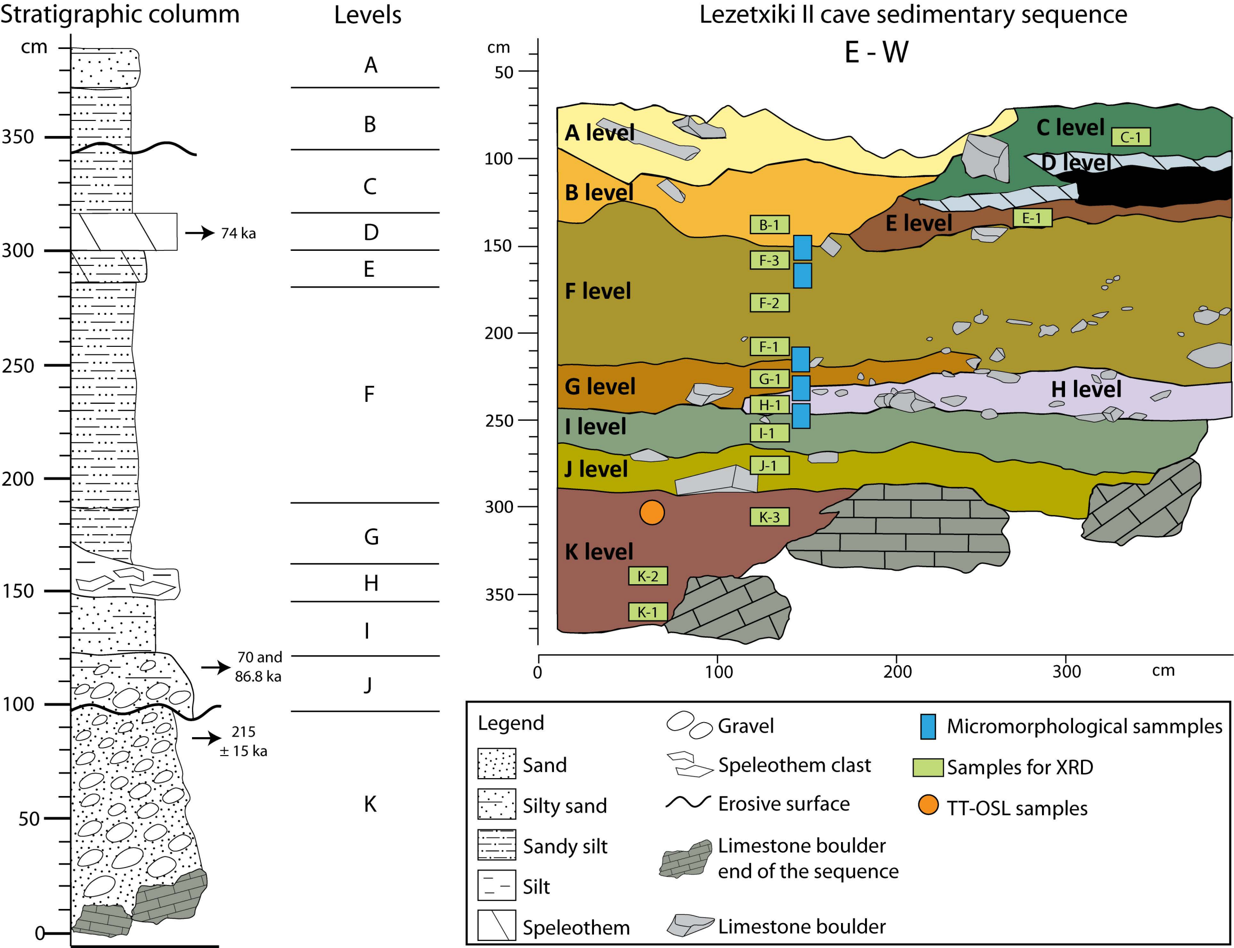

Stratigraphic columm
Levels
Lezetxiki II cave sedimentary sequence
E - W
cm
350
300
250
200
150
100
50
0
74 ka
70 and 86.8 ka
215 ± 15 ka
A
B
C
D
E
F
G
H
I
J
K
cm
50
100
150
200
250
300
350
A level
B level
C level
D level
E level
F level
G level
H level
I level
J level
K level
C-1
B-1
E-1
F-3
F-2
F-1
G-1
H-1
I-1
J-1
K-3
K-2
K-1
0
100
200
300
cm
Legend
Sand
Silty sand
Sandy silt
Silt
Speleothem
Gravel
Speleothem clast
Erosive surface
Limestone boulder end of the sequence
Limestone boulder
Micromorphological sammples
Samples for XRD
TT-OSL samples

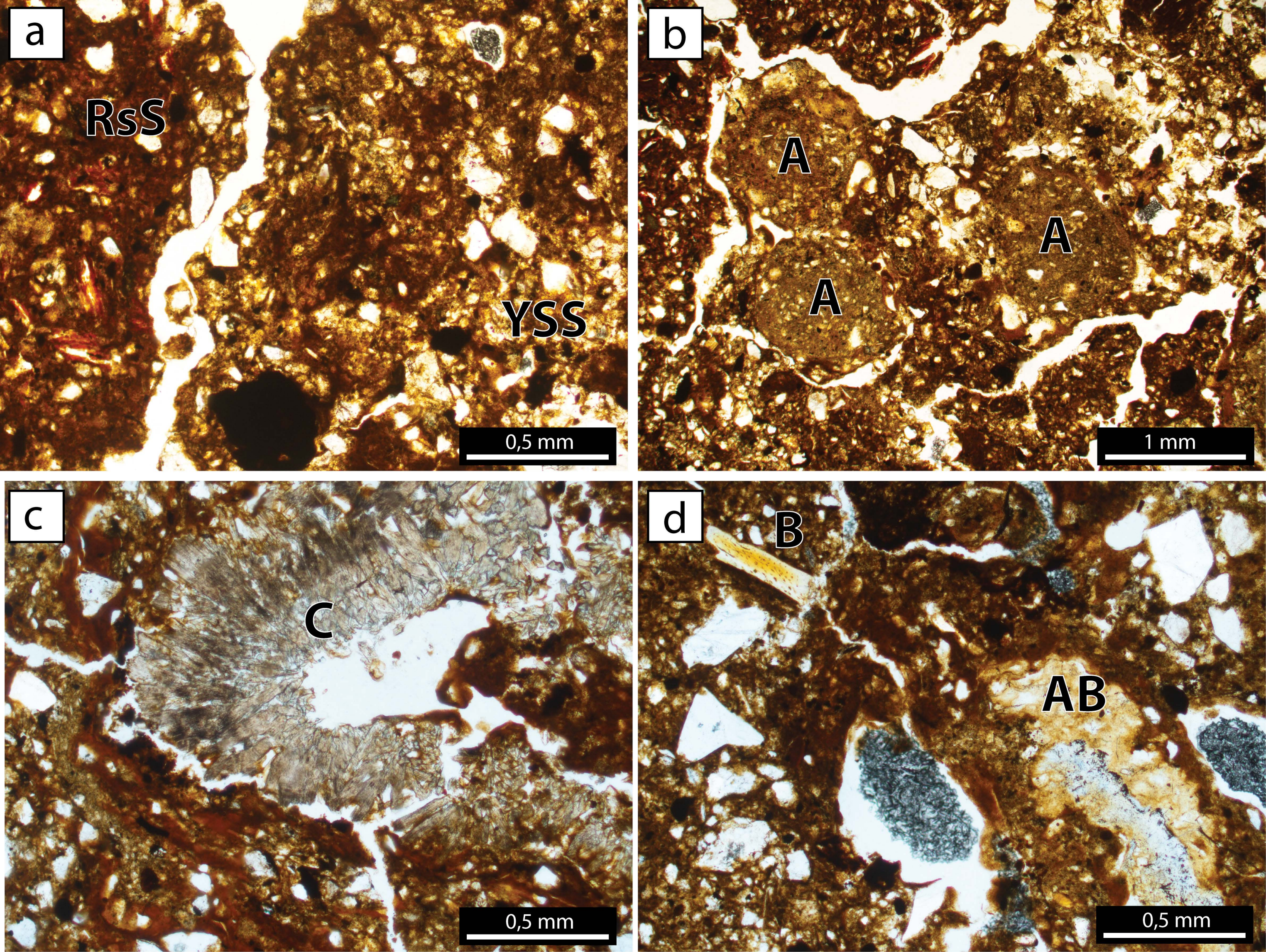
a
RsS
YSS
0,5 mm
b
A
A
A
1 mm
c
C
0,5 mm
d
B
AB
0,5 mm

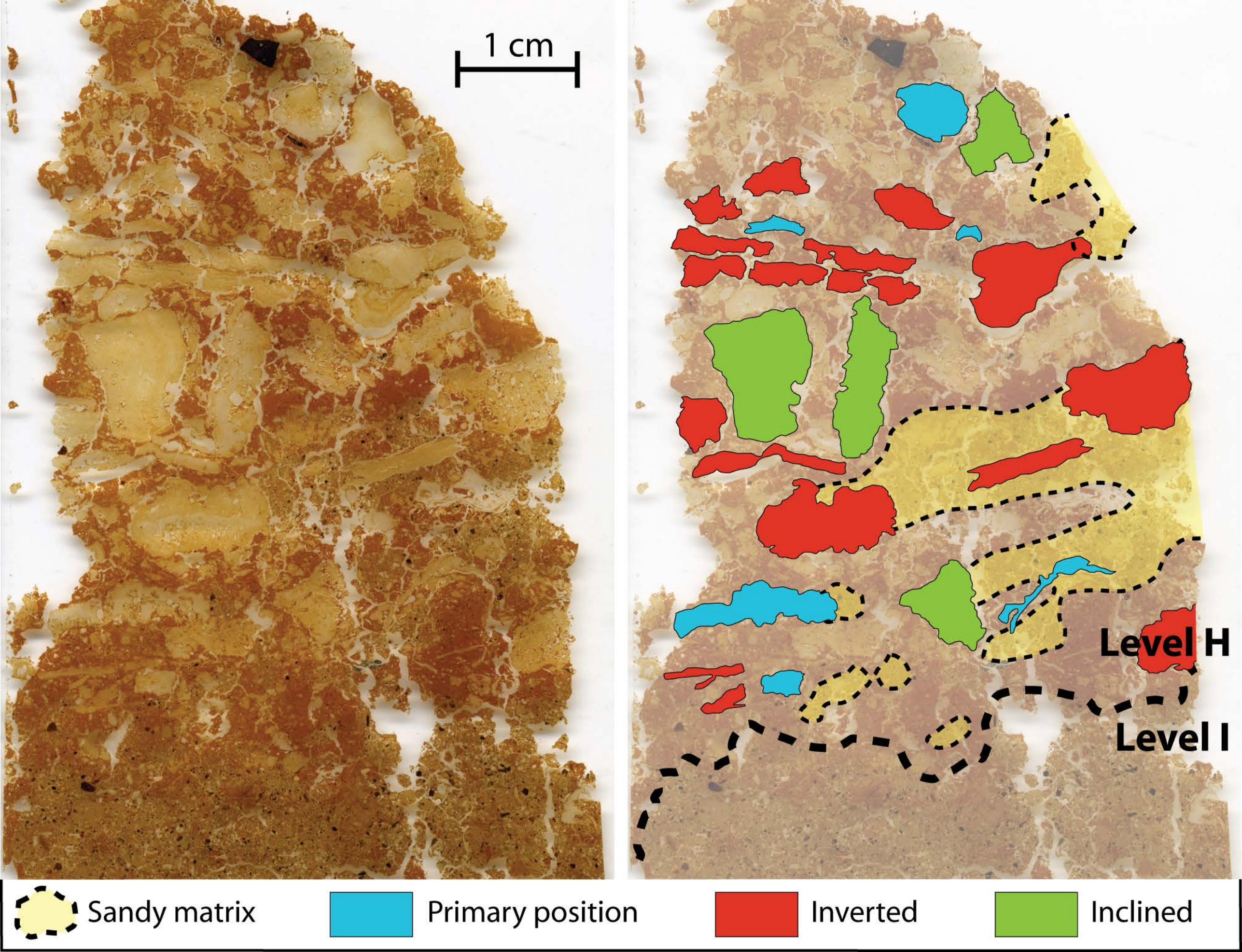
1 cm
Level H
Level I
Sandy matrix
Primary position
Inverted
Inclined

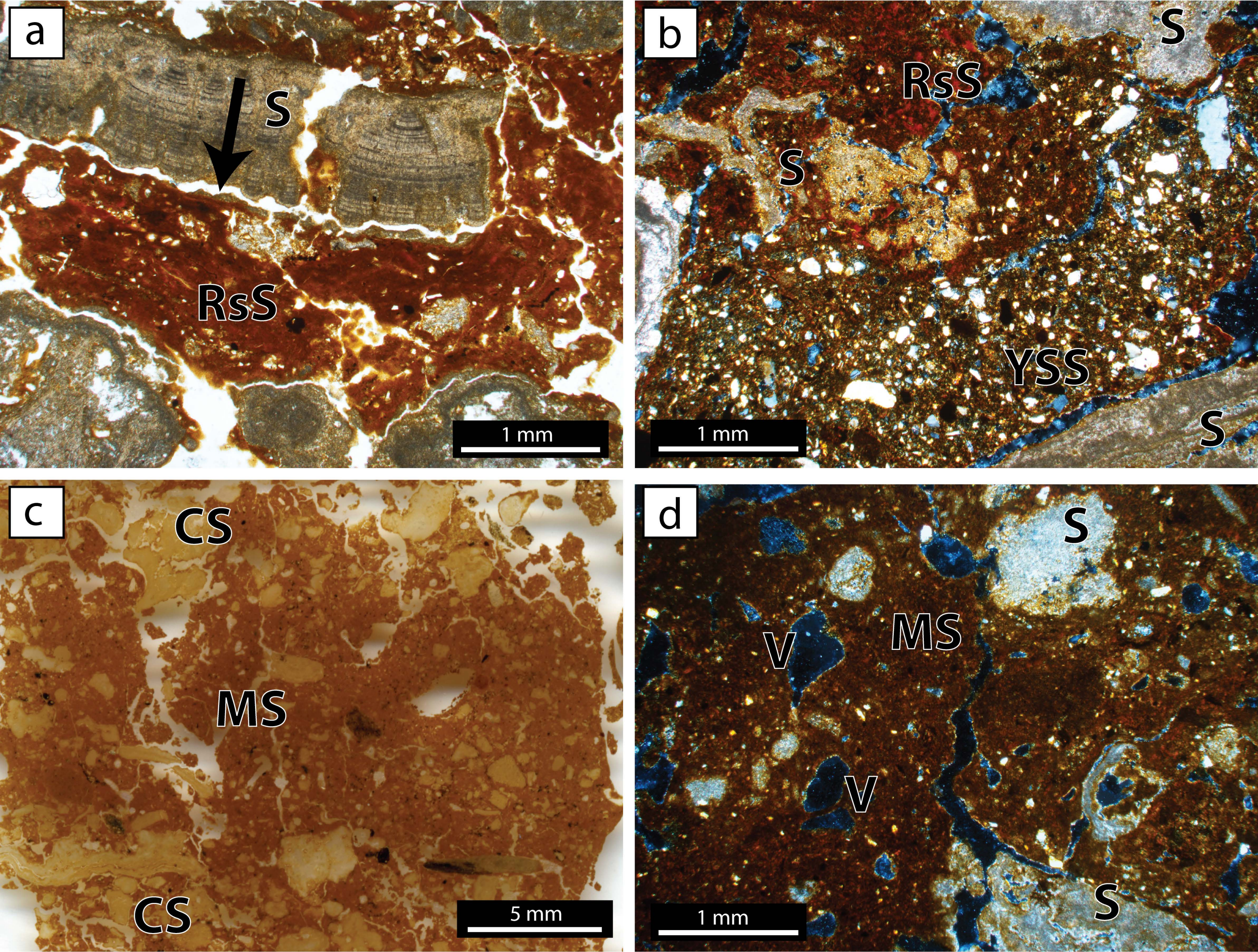
a
S
RsS
1 mm
b
S
RsS
S
YSS
S
1 mm
c
CS
MS
CS
5 mm
d
S
MS
V
V
S
1 mm

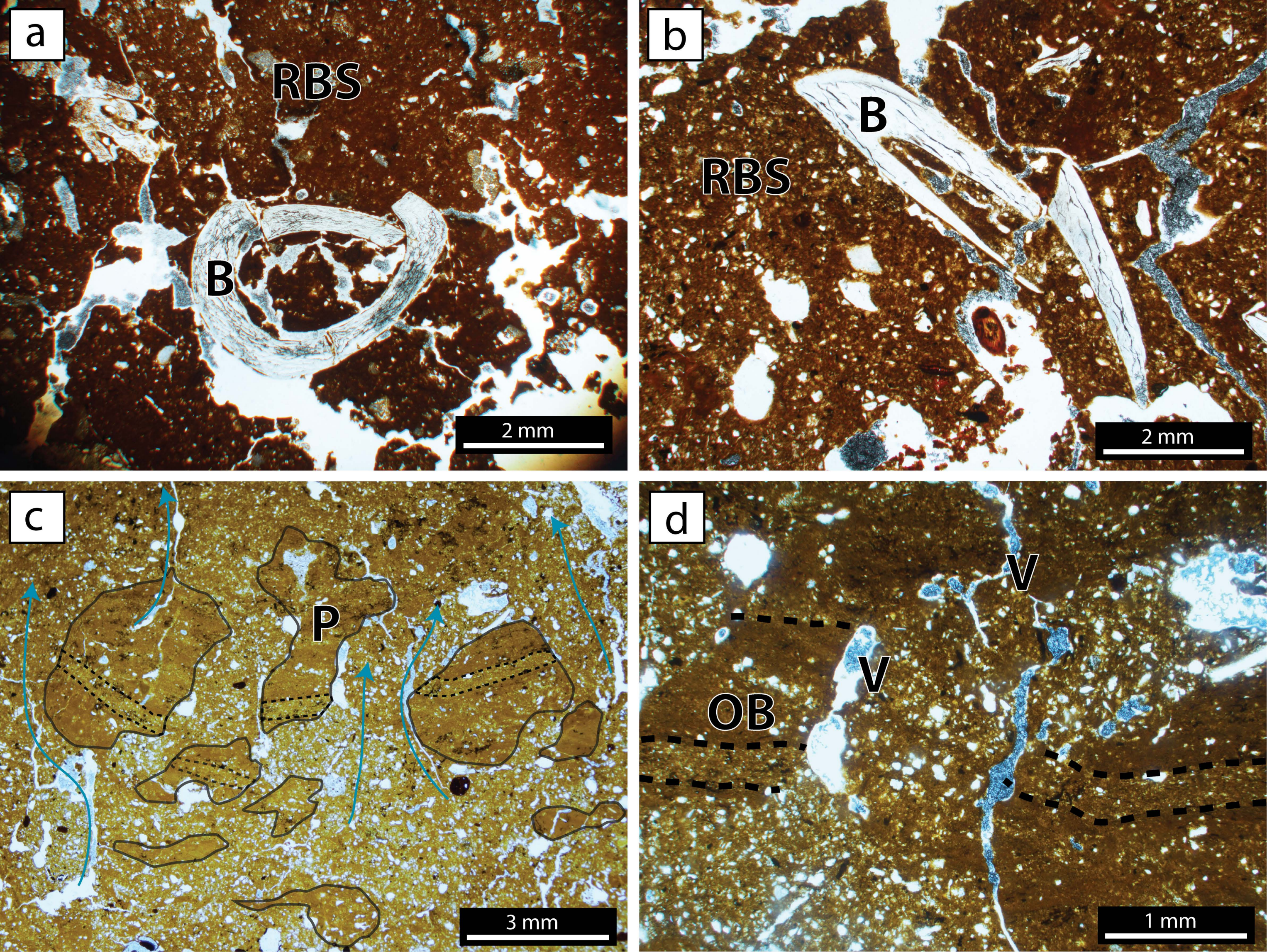
a
RBS
B
2 mm
b
B
RBS
2 mm
c
P
3 mm
d
V
V
OB
1 mm

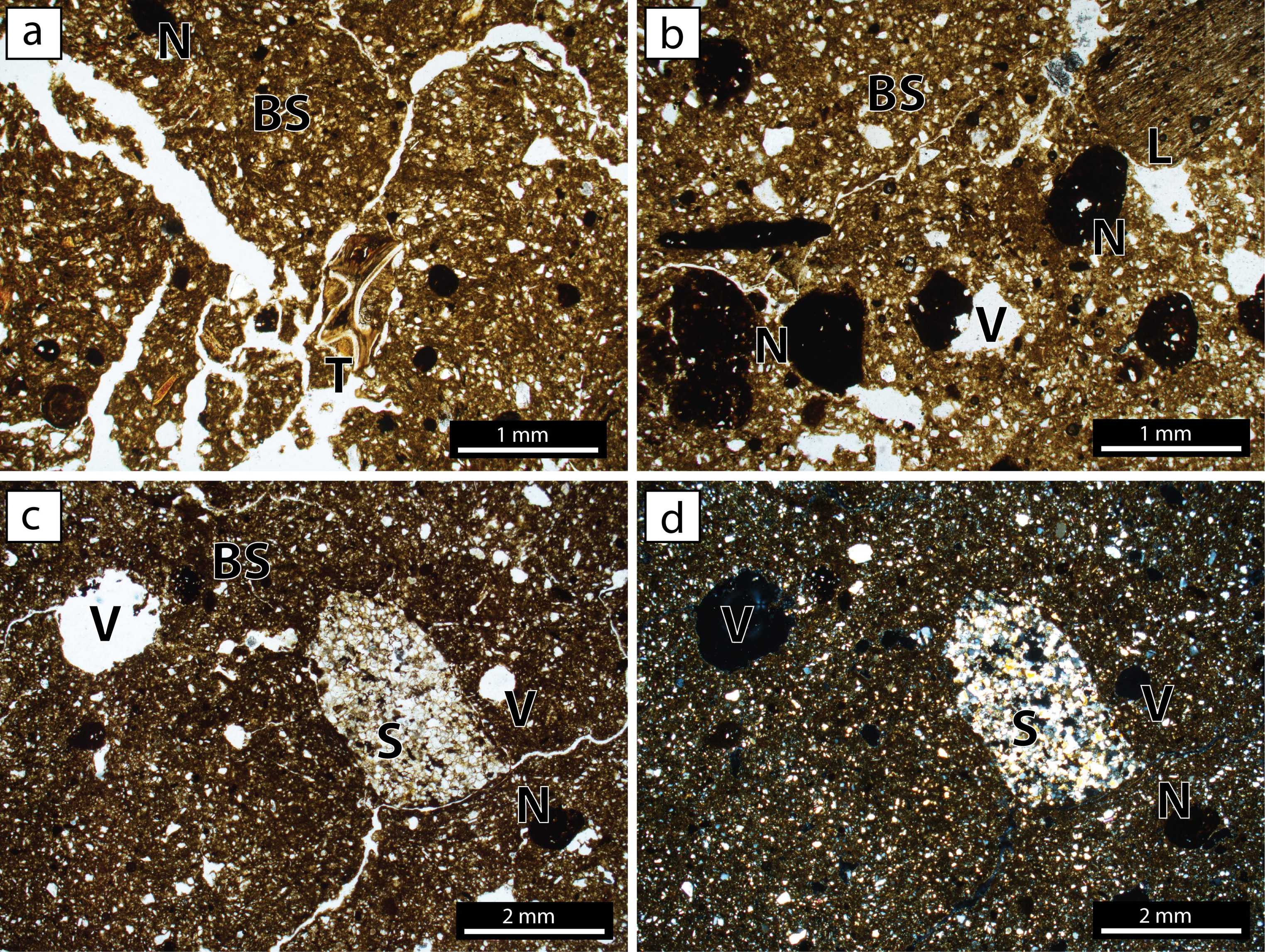

a
N
BS
T
1 mm
b
BS
L
N
N
V
1 mm
c
BS
V
V
S
N
2 mm
d
V
V
S
N
2 mm

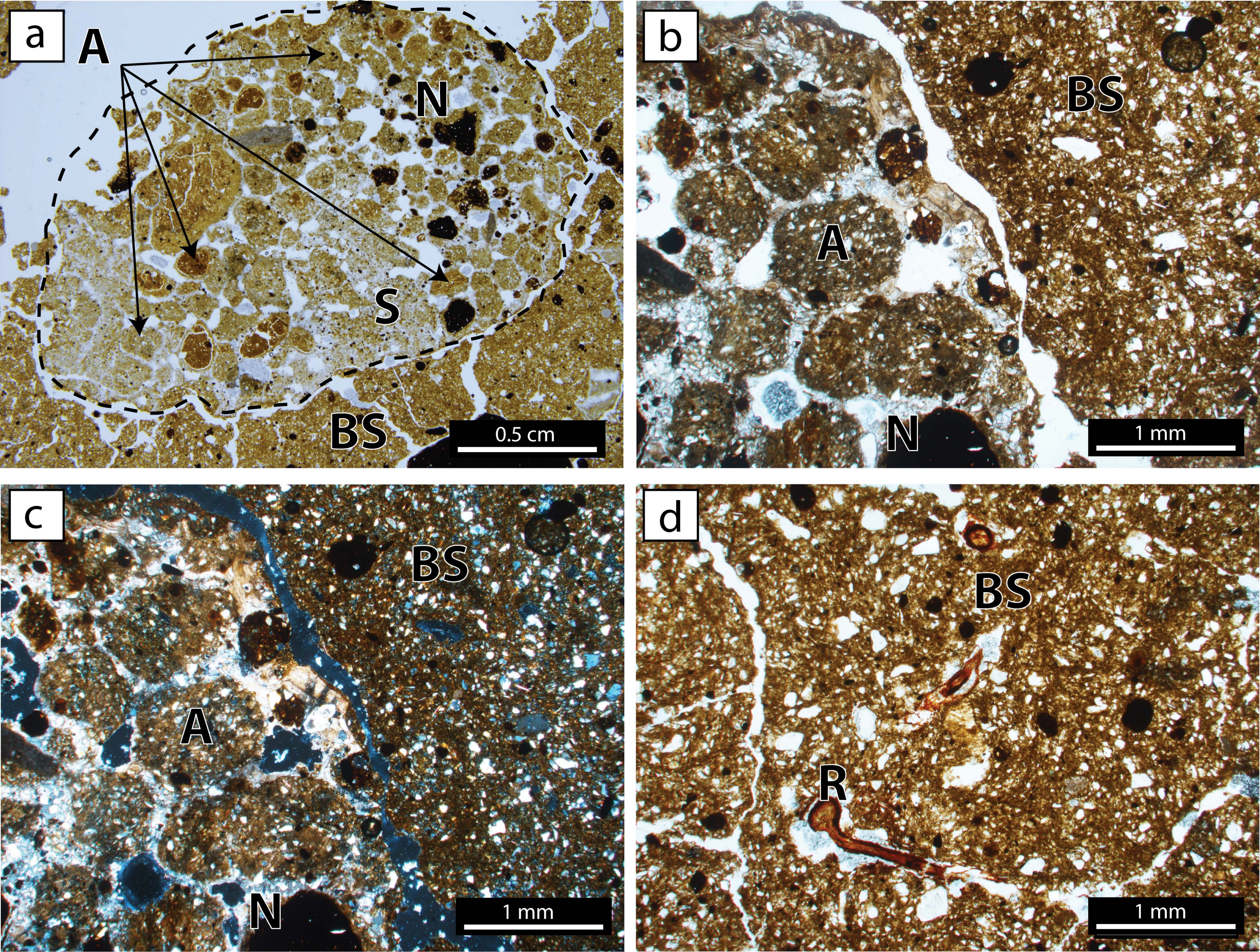
a
A
N
S
BS
0.5 cm
b
BS
A
N
1 mm
c
BS
A
N
1 mm
d
BS
R
1 mm

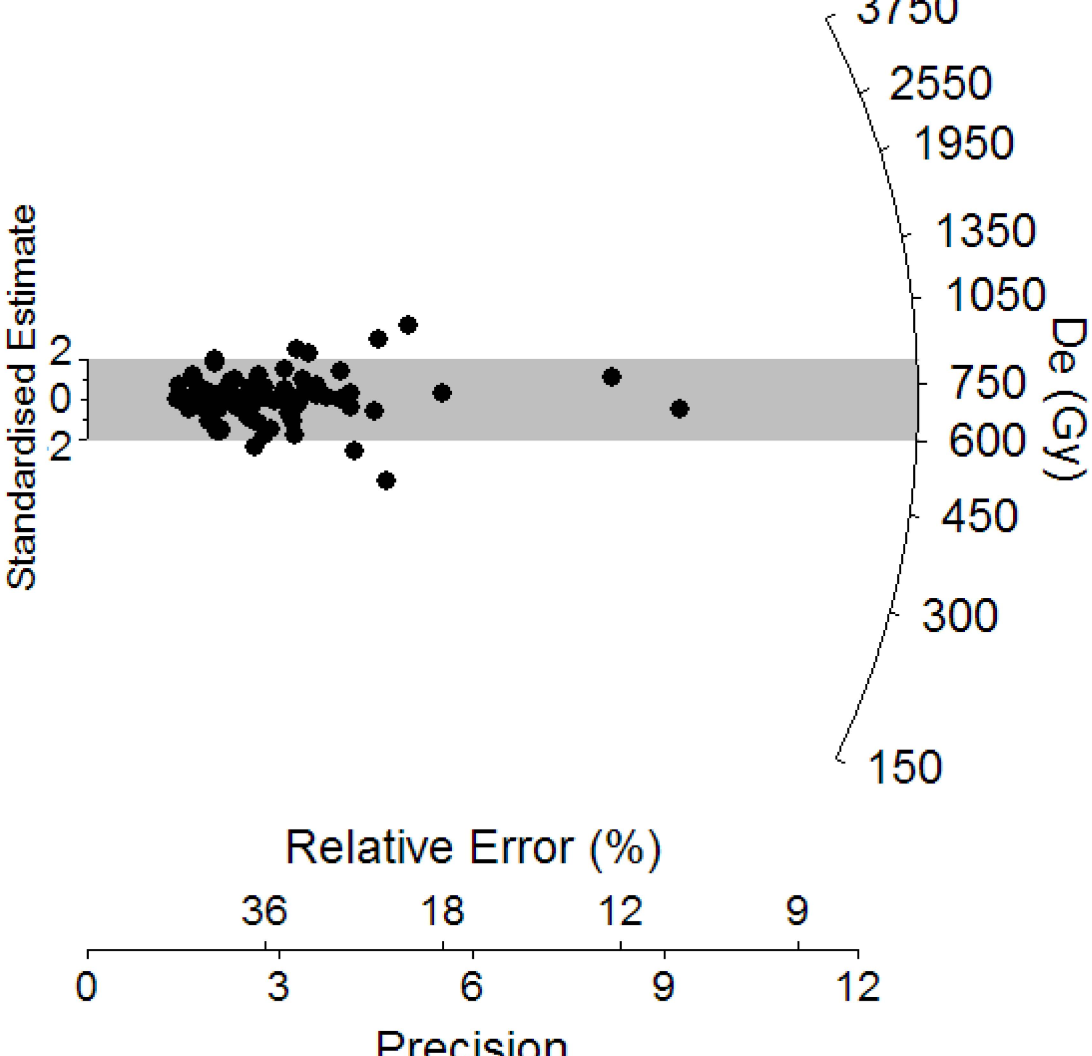

3750
2550
1950
1350
1050
750
600
450
300
150
De (Gy)
Standardised Estimate
2
0
2
Relative Error (%)
36
18
12
9
0
3
6
9
12
Precision

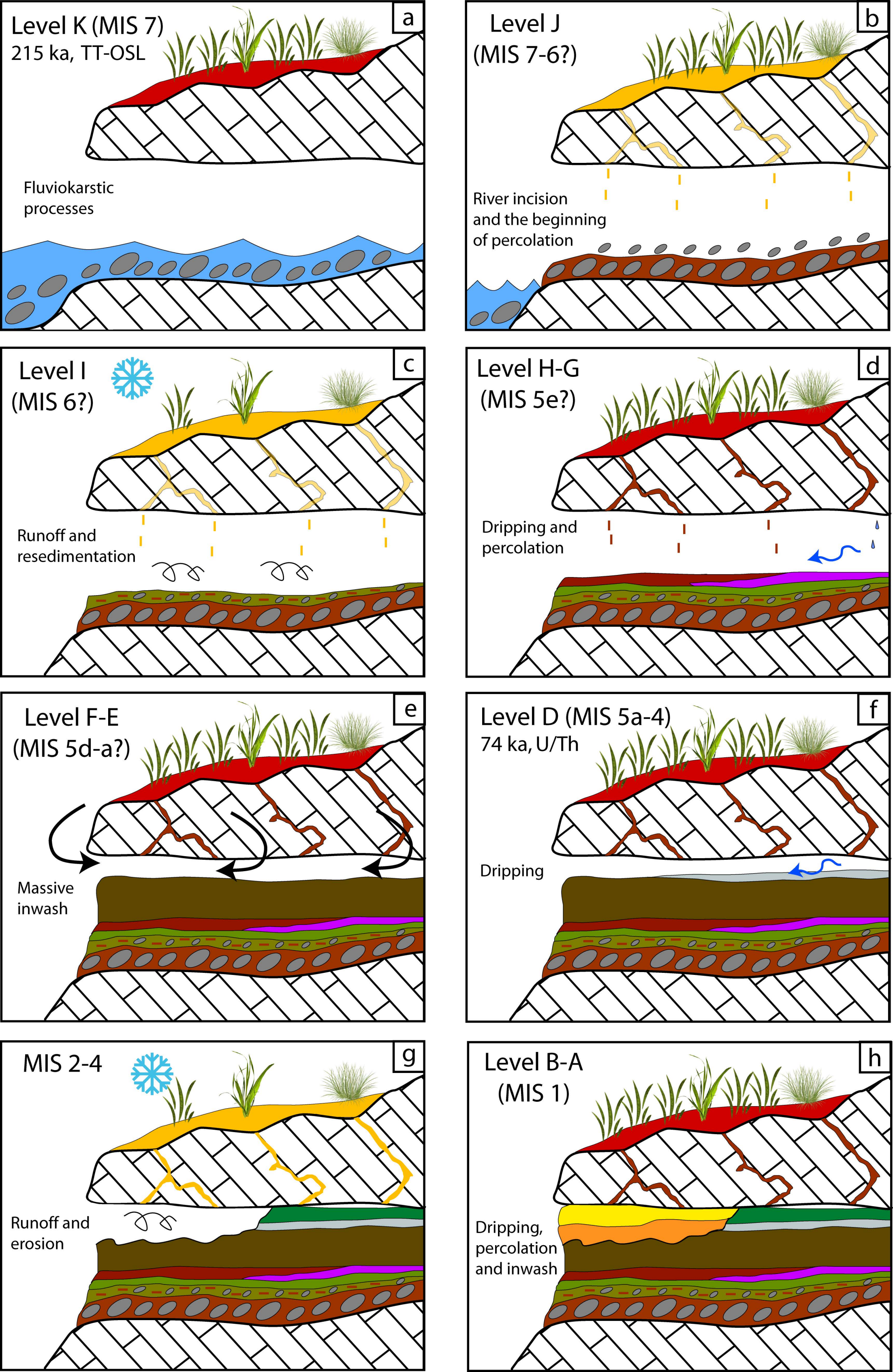

Level K (MIS 7)
215 ka, TT-OSL
a
Fluviokarstic
processes
Level J
(MIS 7-6?)
b
River incision
and the beginning
of percolation
Level I
(MIS 6?)
c
Runoff and
resedimentation
Level H-G
(MIS 5e?)
d
Dripping and
percolation
Level F-E
(MIS 5d-a?)
e
Massive
inwash
Level D (MIS 5a-4)
74 ka, U/Th
f
Dripping
MIS 2-4
g
Runoff and
erosion
Level B-A
(MIS 1)
h
Dripping,
percolation
and inwash

Table 1.

Stratigraphic Level	Level description	Archaeological and paleontological remains
A	Ca. 20-30 cm-thick level, ending laterally against level C. Matrix-supported and consisting of silty sediment with gastropods and some subangular limestone boulders.	No archaeological remains
B	10-40 cm-thick level, lying on an erosive surface. It ends laterally against levels E, D and C. Matrix-supported, consists of massive clayey-silt sediments with some subangular limestone boulders.	Chalcolithic potsherds and lithic industry
C	Ca. 30 cm-thick laterally continuous level that is eroded towards the cave entrance. Matrix-supported, massive silty-clay with gastropods, pieces of flint and anorthic ferruginous nodule fragments.	Aurignacian lithic assemblage
D	Ca. 15 cm-thick speleothem flowstone with the outer part eroded.	No archaeological remains
E	Ca. 10-25 cm-thick, laterally continuous level eroded towards the cave entrance. Matrix-supported massive silty-clay sediment cemented by calcium carbonate.	No archaeological remains
F	Ca. 1 m-thick, laterally continuous, matrix-supported, massive clayey-silt sediment. Coarse fraction components are few quartzite and anorthic ferruginous nodule pebbles, and few subangular limestone boulder.	Numerous faunal remains, especially *Ursus spelaeus* (Villaluenga et al., 2012)
G	Ca. 25 cm-thick, laterally disappearing towards the cave interior. Matrix-supported, massive silty-clay sediment. The coarse fraction consist in few subangular limestone boulders.	Mousterian lithic assemblage. Faunal remains, notably *Muscardinus avellanarius* (Garcia-Ibaibarriaga et al., 2015)
H	Ca. 25 cm-thick level, laterally disappearing towards the cave entrance. Clast-supported deposit, consist on poorly sorted granule and pebble of calcite fragments and clayey matrix. Additionally it contains few subangular limestone boulders.	Mousterian lithic assemblage, faunal remains
I	Ca. 20-30 cm-thick, laterally continuous level, matrix-supported, massive silty-sand sediments with anorthic ferruginous nodule fragments. Additionally there is some subangular limestone boulder.	Mousterian lithic assemblage, faunal remains
J	Ca. 20-30 cm-thick, laterally continuous upward-finning sequence, from clast to matrix-supported, lying on an erosive surface. Silty sand matrix with well sorted cobbles and pebbles that consist of rounded allochtonous sandstone and anorthic ferruginous nodules. Additionally there is some subangular limestone boulder.	Some bone fragments, most notably *Sicista betulin*a (Rofes et al., 2012) and *Macaca sylvanus* (Castaños et al., 2011)
K	Ca. 1 m-thick upward-finning sequence of clast-supported conglomerate. Clast are well sorted, varying from cobble to pebble and consisting of rounded allochtonous sandstone and anorthic ferruginous nodules. The level outcrops in the outer part of the cave.	No archaeological remains. Microfaunal remains

Table 2.

Stratigraphic level	Micromorphological description
B	Matrix-supported, displaying massive microstructure, open porphyric coarse-fine (*c/f*) related distribution and undifferentiated b-fabric. The groundmass is BS type. Skeleton grains consist of speleothem fragments (40%), anorthic ferruginous nodules (30%), sandstone lithoclasts (15%) and lutite lithoclasts (15%).
F/B	Gradual, barely perceptible. Appearance of calcite crystals filling some of the fissure porosity.
F	Matrix-supported, displaying a massive and fissure-type microstructure, mainly an open porphyric *c/f* related distribution - also a single spaced porphyric in the upper part of the level -, and undifferentiated b-fabric The groundmass is BS type. Skeleton grains consist of anorthic ferruginous nodules (50%), sandstone lithoclast (20%), lutite lithoclasts (20%) and bone fragments (10%).
G/F	Gradual contact. The groundmass change gradually from RBS to BS, and the proportion of allochthonous components increase.
G	Matrix-supported, displaying a massive microstructure, open porphyric *c/f* related distribution and undifferentiated b-fabric. The groundmass is RBS type. Skeleton grains consist of microfauna bones (40%), anorthic ferruginous nodules (30%), lutite pebbles (20%), and sandstone pebbles (10%).
H/G	Irregular contact marked by the absence of speleothem fragments and the appearance of RBS.
H	Alternation of clast-supported and matrix-supported microfabric. Clast-supported, displaying a massive microstructure, close porphyric *c/f* related distribution and undifferentiated b-fabric. The groundmass is basically RsS, with some YSS (YSS/RsS ratio is 20/80). Skeleton grains consist of sub-angular flowstone fragments (95%), microfauna bones (3%) and anorthic ferruginous grains (2%). Matrix-supported, displaying an open porphyric *c/f* related distribution and undifferentiated b-fabric. The groundmass is RsS (100%). Skeleton grains are speleothem fragments (100%).
I/H	Highly irregular contact marked by the appearance of speleothem fragments and RsS.
I	Matrix-supported, displaying a massive microstructure, single spaced porphyric *c/f* related distribution and undifferentiated b-fabric. The groundmass present YSS and RsS irregularly mixed (YSS/RsS ratio is 55/45). Skeleton grains are rounded rip-up clasts (50%), anorthic ferruginous nodules (25%) and lutite litoclasts (25%).

Table 3.

Stratigraphic Level	Bulk sample (%)						Clay minerals (%)		
	Qtz	**Cal**	**C.M.**	**Fsp**	**Hap**	**Gt**	**Vrm**	**Ill**	**Kln**
B	42.4	5.9	43.4	7.4	0.4	0.5	21	69	10
C	41.9	5.8	42.2	9.3	0.4	0.5	14	79	7
E	23.0	46.4	25.4	4.1	0.5	0.6	11	80	9
F3	45.1	0.1	47.0	6.4	0.6	0.8	14	76	10
F2	457	0.1	48.3	4.7	0.5	0.7	18	71	11
F1	45.7	0.2	46.9	5.7	1.0	0.6	16	75	9
G	42.5	0.1	48.8	6.5	1.1	1.1	23	68	9
H	17.8	46.1	28.5	5.5	0.9	1.2	30	59	11
I	44.0	0.4	47.2	6.7	0.5	1.2	12	82	6
J	42.5	0.2	49.3	6.0	0.8	1.2	17	73	10
K3	36.4	0.1	48.6	13.1	0.6	1.2	13	82	5
K2	38.8	0.1	48.2	11.6	0.5	0.7	6	86	8
K1	38.5	0.1	50.5	9.4	0.5	1.0	5	90	5

Table 4.

Sample	Layer	Grain size (µm)	Measured water content [a]	Environmental dose rate (Gy/ka)				Equivalent dose (D_e) data				TT-OSL age (ka) [f,k]
				Beta dose rate [b,c]	Gamma dose rate [c,d]	Cosmic dose rate [e]	Total dose rate [f,g]	No. of grains [h]	Overdis-persion (%) [i]	Age Model [j]	D_e (Gy) [f]	
LZ12-6	K	90 – 125	17 ± 2	1.94 ± 0.1	1.27 ± 0.05	0.06 ± 0.01	3.29 ± 0.15	84 / 2300	25 ± 6	CAM	710.0 ± 34.8	215.7 ± 15.1

[a] Field water content, expressed as % of dry mass of mineral fraction, with an assigned relative uncertainty of ±10%.
[b] Calculated on dried and powdered sediment samples using a Risø GM-25-5 low-level beta counter.
[c] Specific activities and radionuclide concentrations have been converted to dose rates using the conversion factors given in Guérin et al. (2011), making allowance for beta-dose attenuation (Mejdahl, 1979; Brennan, 2003).
[d] Calculated from *in situ* measurements made at each sample position with a NaI:Tl detector, using the 'energy windows' approach (e.g., Arnold et al., 2012).
[e] Cosmic-ray dose rates were calculated using the approach of Prescott and Hutton (1994), and assigned a relative uncertainty of ±10%.
[f] Mean ± total uncertainty (68% confidence interval), calculated as the quadratic sum of the random and systematic uncertainties.
[g] Includes an internal dose rate of 0.03 Gy/ka with an assigned relative uncertainty of ±30%.
[h] Number of D_e measurements that passed the SAR rejection criteria of Arnold et al. (2014) and were used for D_e determination / total number of grains analysed.
[i] The relative spread in the D_e dataset beyond that associated with the measurement uncertainties for individual D_e values, calculated using the central age model (CAM) of Galbraith et al. (1999).
[j] The CAM was used to calculate the final D_e of as this sample had a low overdispersion value, consistent with that observed in 'ideal' well-bleached and unmixed sample from similar settings (Arnold and Roberts, 2009; Arnold et al., 2014; Demuro et al., 2014).
[k] Total uncertainty includes a systematic component of ±2% associated with laboratory beta-source calibration.